

***International Collaborations
Activities on Disposal in
Argillite R&D: Bentonite
Barrier Characterization
Studies and Modeling
Investigations***

Fuel Cycle Research & Development

***Prepared for
U.S. Department of Energy***

***Spent Fuel Waste Science
and Technology***

***Carlos F. Jové Colón,
Tuan Ho,
Eric Coker,
Teklu Hadgu,
Carlos M. Lopez,
Jessica Kruichak
Melissa Mills,
Amanda Sanchez***

***Sandia National Laboratories
May 1, 2020***

SAND2020-14037 R



DISCLAIMER

This information was prepared as an account of work sponsored by an agency of the U.S. Government. Neither the U.S. Government nor any agency thereof, nor any of their employees, makes any warranty, expressed or implied, or assumes any legal liability or responsibility for the accuracy, completeness, or usefulness, of any information, apparatus, product, or process disclosed, or represents that its use would not infringe privately owned rights. Reference herein to any specific commercial product, process, or service by trade name, trade mark, manufacturer, or otherwise, does not necessarily constitute or imply its endorsement, recommendation, or favoring by the U.S. Government or any agency thereof. The views and opinions of authors expressed herein do not necessarily state or reflect those of the U.S. Government or any agency thereof.

Sandia National Laboratories is a multimission laboratory managed and operated by National Technology and Engineering Solutions of Sandia, LLC, a wholly owned subsidiary of Honeywell International, Inc., for the U.S. Department of Energy's National Nuclear Security Administration under contract DE-NA-0003525.

This page is intentionally blank.

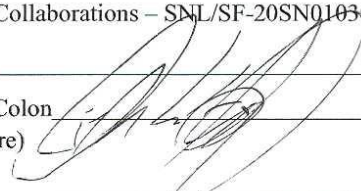
ACKNOWLEDGEMENTS

The authors acknowledge our gratitude to Yifeng Wang (SNL), Charles R. Bryan (SNL), Jonny Rutqvist (LBNL), Liange Zheng (LBNL), Jens Birkholzer (LBNL), Ed Matteo (SNL), William Spezialetti (DOE NE-81), Prasad Nair (DOE NE-81), Mark Tynan (DOE NE-81), and Tim Gunter (DOE NE-81) for their helpful discussions and contributions on various topics covered in this report. We also express our gratitude to Dr. Teruki Iwatsuki (JAEA) for sharing technical information from the GREET experiment at the Mizunami URL Site in Japan. This work was supported by the DOE-NE SFWD office.

APPENDIX E
NFCSC DOCUMENT COVER SHEET¹

Name/Title of Deliverable/Milestone/Revision No. : International Collaborations Activities on Disposal in Argillite R&D:

Bentonite Barrier Characterization Studies and Modeling Investigations

Work Package Title and Number Argillite International Collaborations – SNL/SF-20SN01030109
 Work Package WBS Number 1.08.01.03.01
 Responsible Work Package Manager Carlos F. Jove Colon
 (Name/Signature) 

Date Submitted

Quality Rigor Level for Deliverable/Milestone ²	<input type="checkbox"/> QRL-1	<input type="checkbox"/> QRL-2	<input checked="" type="checkbox"/> QRL-3	<input type="checkbox"/> QRL-4
	<input type="checkbox"/> Nuclear Data			Lab QA Program ³

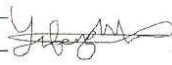
This deliverable was prepared in accordance with Sandia National Laboratories _____
 (Participant/National Laboratory Name)

QA program which meets the requirements of
 DOE Order 414.1 NQA-1 Other

This Deliverable was subjected to:

<input checked="" type="checkbox"/> Technical Review	<input type="checkbox"/> Peer Review
Technical Review (TR)	Peer Review (PR)
Review Documentation Provided	Review Documentation Provided
<input type="checkbox"/> Signed TR Report or,	<input type="checkbox"/> Signed PR Report or,
<input type="checkbox"/> Signed TR Concurrence Sheet or,	<input type="checkbox"/> Signed PR Concurrence Sheet or,
<input checked="" type="checkbox"/> Signature of TR Reviewer(s) below	<input type="checkbox"/> Signature of PR Reviewer(s) below

Name and Signature of Reviewers

Yifeng Wang  _____

NOTE 1: Appendix E should be filled out and submitted with the deliverable. Or, if the PICS:NE system permits, completely enter all applicable information in the PICS:NE Deliverable Form. The requirement is to ensure that all applicable information is entered either in the PICS:NE system or by using the NFCSC Document Cover Sheet.

- In some cases there may be a milestone where an item is being fabricated, maintenance is being performed on a facility, or a document is being issued through a formal document control process where it specifically calls out a formal review of the document. In these cases, documentation (e.g., inspection report, maintenance request, work planning package documentation or the documented review of the issued document through the document control process) of the completion of the activity, along with the Document Cover Sheet, is sufficient to demonstrate achieving the milestone.

NOTE 2: If QRL 1, 2, or 3 is not assigned, then the QRL 4 box must be checked, and the work is understood to be performed using laboratory QA requirements. This includes any deliverable developed in conformance with the respective National Laboratory / Participant, DOE or NNSA-approved QA Program.

NOTE 3: If the lab has an NQA-1 program and the work to be conducted requires an NQA-1 program, then the QRL-1 box must be checked in the work Package and on the Appendix E cover sheet and the work must be performed in accordance with the Lab's NQA-1 program. The QRL-4 box should not be checked.

This page is intentionally blank

Table of Contents

Table of Contents	7
Acronym List	11
I. Introduction	12
II. FEBEX-DP	13
III. Thermal (TGA/DSC) Analyses	16
IV. Water transport mechanism in clay interlayer during the dehydration	23
V. FEBEX Bentonite Interactions with FeCl ₂ Solution	25
Experimental Procedure	26
Experiment 1 (“Soaked”): XRD and ICP-OES Analyses	26
Experiment 2 (Heated): XRD and ICP-OES Analyses	29
Discussion	33
VI. DECOVALEX-2019 Task C: GREET (Groundwater REcovery Experiment in Tunnel), Mizunami URL, Japan.....	33
Closure Test Drift (CTD): 3D H-C Model of Shotcrete Liner Interactions	33
VII. Conclusions	46
VIII. FY21 Work.....	47
IX. References	47
X. APPENDIX A	51

Table of Figures

Figure 1. Schematic layout of the FEBEX “in-situ” field test after the first partial dismantling showing the configuration of heater #2 at the GTS URL	14
Figure 2. Schematic configuration of sampling zones for the FEBEX-DP project	15
Figure 3. Schematic diagram of sampling locations for the FEBEX-DP dismantling of section 49.	16
Figure 4. TGA/DSC curves as a function of time (minutes) for water adsorption/desorption cycles at 60°C for sample BG-C-49-3 away from the heater surface.....	18
Figure 5. Elapsed time for dehydration for the appearance of the second peak as a function of hydration duration in cyclical TGA/DSC studies of water adsorption/desorption	19
Figure 6. TGA, DTA, and DSC curves as a function of time for water adsorption/desorption cycles at 60°C for the 2 μm bentonite sample.	20
Figure 7. TGA, DTA, and DSC curves as a function of time for water adsorption/desorption cycles at 60°C for the 38 μm bentonite sample.	21
Figure 8. TGA and DSC curves as a function of time for water adsorption/desorption cycles at 60°C for the 75 μm bentonite sample.	22
Figure 9. Simulation system used to study the dehydration process of Na-Montmorillonite.	24
Figure 10. Number of atoms in the MD simulation box as a function of time	24
Figure 11. Calculated XRD pattern for the Na-MMT structures reported in snapshots A, B, and C shown in Figure 10.	25
Figure 12. XRD patterns of “Soaked” experiments	27
Figure 13. Fe, Si, Mg, and Ca concentrations in supernatant and rinse solutions for “Soaked” experiments.....	28
Figure 14. Al, Na, and K concentrations in supernatant and rinse solutions for the “Soaked” experiments.....	29
Figure 15. XRD spectra of FEBEX bentonite for the Experiment 2 (Heated).....	30
Figure 16. XRD spectra for FEBEX bentonite samples (Baseline and close to the heater)	31
Figure 17. Fe, Si, Ca, Mg, Al, and Na concentrations for the supernatant in Experiment 2 (Heated).	32
Figure 18. Diagrammatic picture of the closure test drift (CTD) at the Mizunami URL site, Japan.....	34
Figure 19. Vertical slice along the axis of the tunnel showing the CTD region (light green) and inclined drift (light blue).....	35
Figure 20. Mesh refinement showing shotcrete plug and lining around the CTD.	35
Figure 21. 3D domain representation of upscaled permeability field for DFN Realization 2.	36
Figure 22. 3D domain representation of upscaled porosity field for DFN Realization 2.	36
Figure 23. Schematic figure showing a YZ of the model domain in the PFLOTTRAN reactive transport simulation of the CTD	37
Figure 24. Predicted pH of the PFLOTTRAN 3D reactive transport model of the CTD and surrounding host rock.	39

Figure 25. Measured and predicted pH and Na ⁺ concentration in moles/L profiles at the midpoint region of the CTD and shotcrete thickness of 10 cm.....	41
Figure 26. Measured and predicted Ca ⁺⁺ and Cl ⁻ concentration profiles in moles/L at the midpoint region of the CTD and shotcrete thickness of 10 cm.....	42
Figure 27. Measured and predicted pH and Na ⁺ concentration in moles/L profiles at the midpoint region of the CTD and shotcrete thickness of 20 cm.....	44
Figure 28. Measured and predicted Ca ⁺⁺ and Cl ⁻ concentration profiles in moles/L at the midpoint region of the CTD and shotcrete thickness of 20 cm.....	45
Figure A-1. TGA/DSC curves as a function of time (minutes) for water adsorption/desorption cycles at 60°C for unheated (baseline) FEBEX bentonite	52
Figure A-2. TGA/DSC curves as a function of time (minutes) for water adsorption/desorption cycles at 60°C for FEBEX-DP bentonite samples BG-C-49-1 and BG-C-49-3.....	53
Figure A-3. Volumetric water sorption/desorption isotherms obtained at 20°C for samples BG-C-49-1 and BG-C-49-3.	54
Figure A-4. TGA/DSC curves as a function of time (minutes) for water adsorption/desorption cycles at 60°C for FEBEX-DP bentonite samples B-C-49-7 and B-C-49-11.	55
Figure A-5. Volumetric water sorption/desorption isotherms obtained at 20°C for samples BG-C-49-7 and BG-C-49-11.	56
Figure A-6. TGA/DSC curves as a function of time (minutes) for water adsorption/desorption cycles at 60°C for FEBEX-DP bentonite samples B-C-49-8 and B-C-49-12.	57
Figure A-7. Volumetric water sorption/desorption isotherms obtained at 20°C for samples BG-C-49-8 and BG-C-49-12	58
Figure A-8. TGA/DSC curves as a function of time (minutes) for water adsorption/desorption cycles at 60°C for FEBEX-DP bentonite samples BM-D-49-3 and BM-D-49-(1,2,3)..	59
Figure A-9. Volumetric water sorption/desorption isotherms obtained at 20°C for samples BM-D-49-3 and BM-D-49-(1,2,3).	60

REVISION HISTORY

Acronym List

CTD	Closure Test Drift
DECOVALEX	DEvelopment of COupled models and their VALidation against EXperiments
DSC	Differential Scanning Calorimetry
DOE	Department of Energy
DOE-NE	DOE Office of Nuclear Energy
EBS	Engineered Barrier System
EDS	Energy Dispersive Spectroscopy
EDZ	Excavated Disturbed Zone
FEBEX-DP	Full-scale Engineering Barrier Experiments – Dismantling Project
GREET	Groundwater REcovery Experiment in Tunnel
GTS	Grimsel Test Site
H-C	Hydro-Chemical
ICP-OES	Inductively Coupled Plasma Optical Emission Spectroscopy
JAEA	Japan Atomic Energy Agency
MC	Monte Carlo
MD	Molecular Dynamics
mSEM	Multi (Beam) – Scanning Electron Microscopy
OPC	Ordinary Portland Cement
R&D	Research & Development
RH	Relative Humidity
SEM	Scanning Electron Microscopy
SF	Spent Fuel
SFWD	Spent Fuel and Waste Disposition
SNL	Sandia National Laboratories
TGA	Thermo-Gravimetric Analysis
THC	Thermal-Hydrological-Chemical
THMC	Thermal-Hydrological-Mechanical-Chemical
TST	Transition State Theory
TUL	Technical University of Liberec
URL	Underground Research Laboratory
XRD	X-ray Diffraction
XRF	X-ray Fluorescence
μ -XRF	micron X-ray Fluorescence

I. Introduction

This interim report is an update of the report Jove Colon et al. (2019; M4SF-19SN010301091) describing international collaboration activities pertaining to FEBEX-DP and DECOVALEX19 Task C projects. Although work on these two international repository science activities is no longer continuing by the international partners, investigations on the collected data and samples is still ongoing. Descriptions of these underground research laboratory (URL) R&D activities are given in Jové Colón et al. (2018; 2019) but will be repeated here for completeness. The 2019 status of work conducted at Sandia National Laboratories (SNL) on these two activities is summarized along with other international collaboration activities in Birkholzer et al. (2019).

The FEBEX-DP dismantling of heater #2 (see Fig. 1; Section II) was performed during 2015 involving the careful retrieval of (FEBEX) bentonite barrier material samples from the remaining sections of the FEBEX “in situ test” at the Grimsel test site (GTS) URL, Switzerland, after 18+ years of heating (García-Siñeriz et al., 2016; Martínez et al., 2016). The disassembling activity involved sampling of the barrier bentonite, steel liner, sensors, embedded metallic components (e.g., metal coupons), and near-field sections with tracer components. Participation in the FEBEX-DP project not only allows international partners access to the monitoring data but also to samples collected during the dismantling stage for *post-mortem* characterization of barrier materials. Birkholzer et al. (2017) describes previous work on bentonite-cement interfaces for FEBEX-DP epoxied overcored samples using micro-X-ray fluorescence (μ -XRF) and Multi-SEM (mSEM) scanning probe methods. Jové Colón et al. (2018) and Birkholzer et al. (2018) describes X-ray Fluorescence (XRF), X-ray diffraction (XRD), and thermogravimetric analyses (TGA/DSC) on FEBEX-DP bentonite samples from Section 49. The FEBEX-DP effort has documented bulk XRF bentonite compositional analyses with distance from the heater for various sampled sections of the engineered barrier system (EBS) (Villar et al., 2017). Samples collected in section 49 experienced the hottest zones of the heater given its location close to the center of the (cylindrical) heater longitudinal axis. Jové Colón et al. (2019) describes the FEBEX-DP bentonite XRF compositional data along with XRD analyses, volumetric adsorption/desorption, and thermogravimetric analysis (TGA/DSC) with controlled hydration/dehydration cycles on bentonite samples collected as a function of distance from the gallery center or heater surface.

The DECOVALEX-2019 Task C involves collaboration with the GREET (Groundwater REcovery Experiment in Tunnel) at the Mizunami URL, Japan, which targets the development of monitoring methodologies of groundwater in granitic rock with applications to HMC simulations (Iwatsuki et al., 2005; Iwatsuki et al., 2015). Some of the goals of GREET is to conduct a facility-scale geochemical characterization study of short- and long-term effects of tunnel excavation activities, impacts on groundwater flow and transport, and influences on groundwater chemistry under ambient tunnel conditions (Iwatsuki et al., 2015). The hydrological and hydrochemical data obtained from these URL activities is then used in the development and evaluation of HC models to support post-closure safety and performance assessments of the repository environment. Jové Colón et al. (2019) and Birkholzer et al. (2019) describes 3D reactive transport (HC) modeling of the closure test drift (CTD) focusing on shotcrete – ground water interactions of the cement liner in the water-filled tunnel. The collected field hydrological and hydrochemical monitoring data as a function of time is used to evaluate barrier material interactions effects on the flooded CTD water chemistry using a coupled-process model with heterogeneous permeability fields of the host rock surrounding the CTD.

The main goals of this report update for each of the international activities are:

- FEBEX-DP:
 - (Section III) Provide additional thermogravimetric analysis (TGA/DSC) with controlled hydration/dehydration cycles on FEBEX-DP bentonite samples of different grain sizes. Bentonite hydration/dehydration state controls swelling and shrinkage phenomena in bentonite.
 - (Section IV) Preliminary results from molecular dynamics (MD) simulation of Na-Montmorillonite (Na-MMT) dehydration focusing on water transport at the smectite interlayer. This modeling effort was motivated by the TGA/DSC and water adsorption isotherm experiments to evaluate mechanism of water transport at the molecular level.
 - (Section V) Experimental work on FEBEX bentonite interaction experiments with an FeCl₂ solution under controlled atmospheric conditions at ambient and elevated temperatures.
- DECOVALEX Task C:
 - (Section VI) Updates on the 3D Reactive transport modeling of the closure test drift (CTD) focusing on shotcrete – ground water interactions of the cement liner in the water-filled tunnel. This simulation effort is part of an inter-comparison exercise between different modeling teams (SNL, JAEA, TUL) participating in this task.

II. FEBEX-DP

The post-closure period will experience high thermal loads that can drive fluid transport and barrier alteration as a result of enhanced interactions with fluids, induced phase transformation, and other potential mineralogical changes in bentonite under variably saturated conditions. Jove Colon et al. (2016) describes the 2D-3D characterization of microcracks in FEBEX-DP shotcrete-bentonite overcore outlining the importance of desiccation/shrinkage processes in bentonite and the nature of pores/voids in shotcrete. Engineered barrier alteration has been assessed by reactive-transport models and geochemical modeling of mineral dissolution and precipitation (Marty et al., 2015; Wilson et al., 2015; Xie et al., 2015). An example is Fe-bentonite interactions which leading to mineral phase changes that could impact swelling capacity in bentonite through alteration to a non-swelling Fe-bearing phase. Also, cation exchange in the bentonite clay could also be impacted through temperature-induced drying and wetting causing variations in the cation exchange capacity (CEC) (Muurinen, 2011). Cation exchange experiments reported by Villar et al. (2017) show that FEBEX-DP bentonite samples collected from sections closest to the heater exhibit higher concentrations of Mg and Ca and low concentrations of exchangeable Na. Further, aqueous extracts for bentonite samples collected in sections close to the heater exhibited higher aqueous concentrations of Mg, Ca, Na, and Cl relative to those sampled farther away from the heater. It should be noted that the aqueous extract process is influenced by ion exchange and solid phase dissolution (Villar et al., 2017). These relatively large changes in the observed aqueous concentration from these tests suggest that bentonites close to the heater were affected by thermal loads therefore inducing changes in the smectite clay phase and potentially their subsequent interactions with fluids. It would then be expected that such effects on bentonite bulk mineralogic and chemical composition would influence overall sorption behavior. Jové Colón et al. (2018, 2019) described X-ray fluorescence (XRF), XRD, and TGA/DSC analyses on bulk FEBEX-DP samples from section 49 corresponding to spatial domains near and far from the surface of heater #2 (see Fig. 2 for sample locations). Fig. 3 shows the radial locations of samples collected in Section 49 considered in this study. Section III describes the focus of the current study which is to expand TGA/DSC analyses to FEBEX-DP bentonite samples of various grain sizes. Also, conduct a more

detailed evaluation of the temporal evolution of hydration/dehydration cycles at constant temperature and relative humidity (RH). Motivated by the thermal studies, MD simulations of montmorillonite dehydration under certain conditions were conducted to describe this process at the molecular scale. These studies are discussed in Section IV. Section V summarizes the preliminary results of FEBEX-DP interaction experiments with FeCl_2 solution.

The FEBEX bentonite is composed of ~93% smectite with 2% quartz, 3% plagioclase, and about 2% cristobalite plus minor accessory phases such as calcite and K-feldspar (Huertas et al., 2000; Missana and García-Gutiérrez, 2007). The extent of the corroded region from the heater steel mesh support surface into the bentonite is rather limited which might explain the relatively low level of Fe alteration into the bentonite, particularly in the hotter zones of the heater.

The XRD data reported in Jové Colón et al. (2018) has been evaluated and compared between samples close to and far from the heater surface and that for unheated FEBEX bentonite. As described in Jové Colón et al. (2018), a salient feature revealed by XRF compositional analyses is the increase in Mg content with decreasing distance from the heater or towards the heater surface (~50 cm from the gallery center). An explanation for the Mg enrichment close to the heater surface is still under investigation. Potential mechanisms to be considered are (1) enhanced cation exchange of Mg from pore solution into smectite and (2) enhancement of Mg content already in smectite through removal of other readily exchangeable cations such as Na^+ .

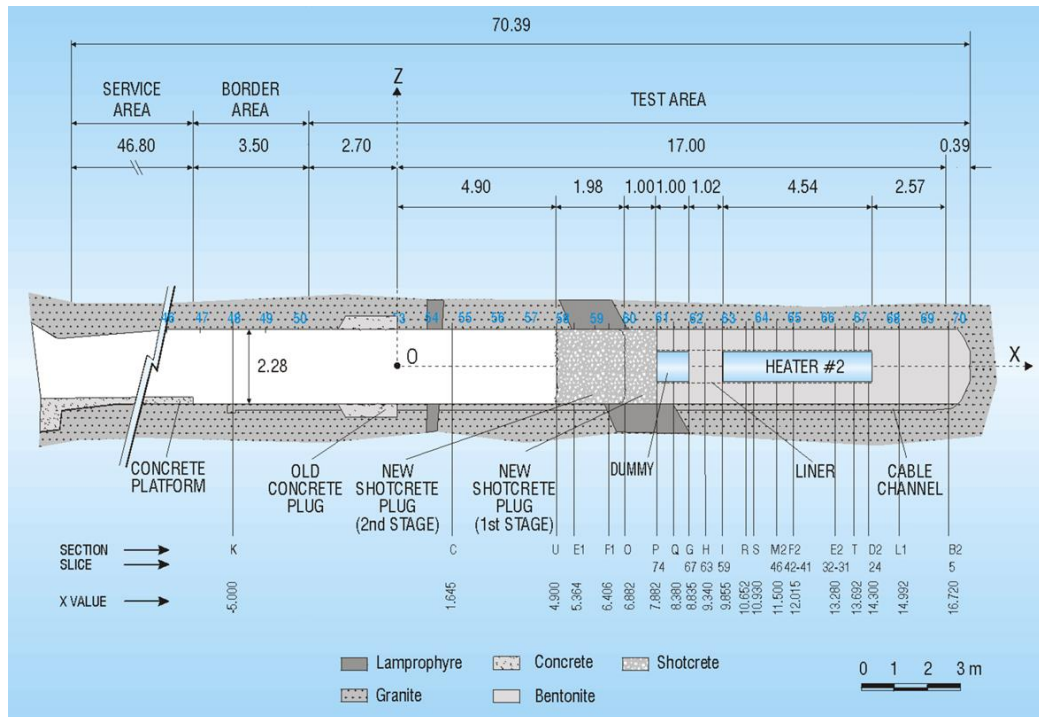


Figure 1. Schematic layout of the FEBEX “in-situ” field test after the first partial dismantling showing the configuration of heater #2 at the GTS URL (García-Siñeriz et al., 2016).

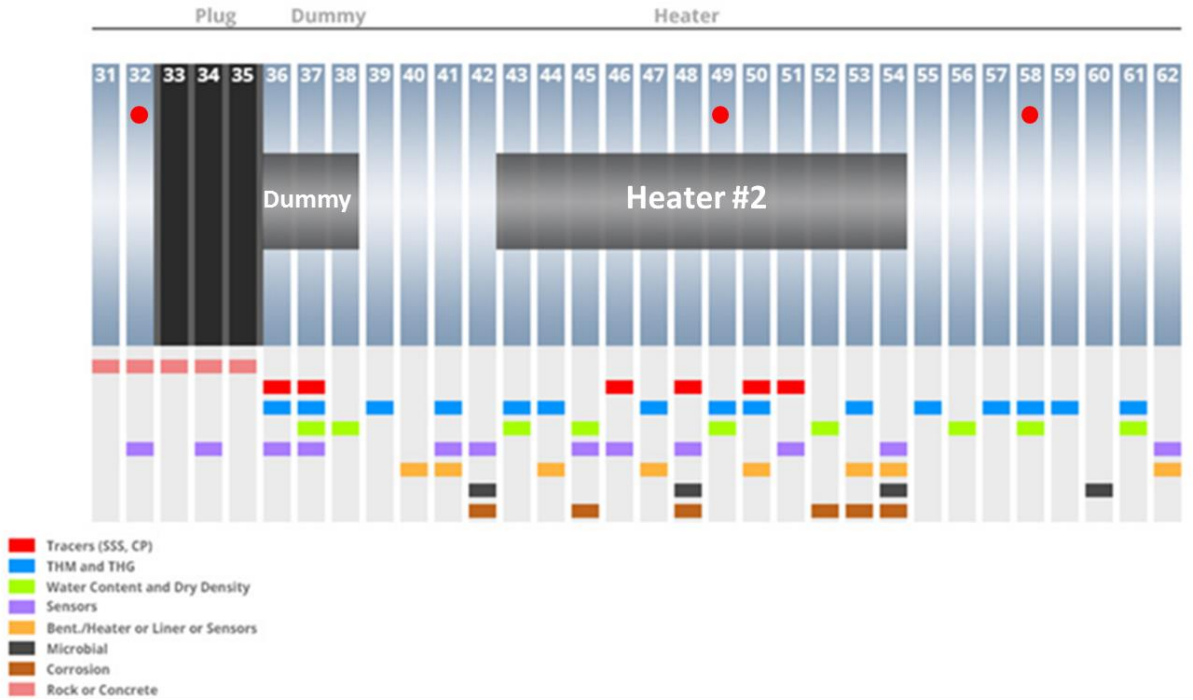


Figure 2. Schematic configuration of sampling zones (indicated by vertical light blue bars) for the FEBEX-DP project. Filled red circles indicate zones for samples obtained by Sandia National Laboratories (SNL). Source: FEBEX-DP website (members area): <http://www.grimsel.com/gts-phase-vi/febex-dp/febex-dp-introduction>.

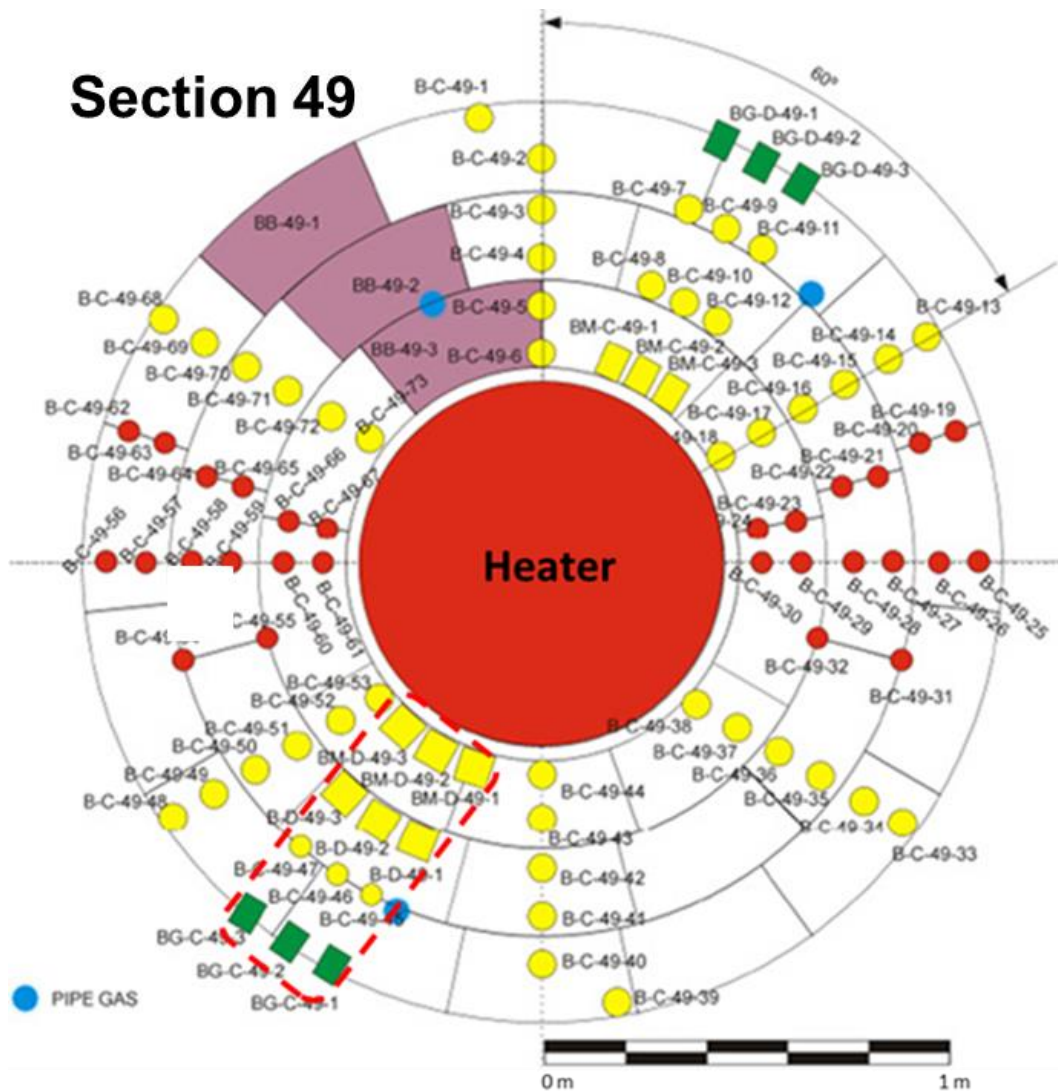


Figure 3. Schematic diagram of sampling locations for the FEBEX-DP dismantling of section 49. See Fig. 2 for section location relative to the heater zone. The red-dashed line delineates the locations of samples analyzed with XRD and XRF (diagram source: FEBEX-DP website (members area): <http://www.grimself.com/gts-phase-vi/febex-dp/febex-dp-introduction.>).

III. Thermal (TGA/DSC) Analyses

Water adsorption/desorption behavior in expansive clay is key to this material swelling phenomena but also to water transport during hydration/dehydration processes. Thermal loads in deep geological nuclear waste repositories control RH conditions in the disposal galleries where bentonite is used as backfill barrier material. Therefore, chemo-mechanical responses and mechanisms of bentonite hydration/dehydration to changes in RH and temperature are crucial to the EBS performance. Cyclical TGA/DSC analyses under controlled RH and temperature supply important information on the kinetics of expansive clay hydration/dehydration and also provides insights on the hysteretic behavior of this process.

For completeness and continuity, TGA/DSC analyses and results reported in Jové Colón et al. (2019) will be retained in this report along with data contained therein included in Appendix A. These

analyses were conducted using a Netzsch STA 449 F3 Jupiter with MHG humidity generator. The analyzed samples are the unheated FEBEX bentonite, BG-C-49-1, BG-C-49-3, B-C-49-7, B-C-49-8, B-C-49-11, B-C-49-12, BM-D-49-3, BM-D-49-1,2,3. Appendix A provide data of adsorption/desorption for bentonite close and far from the heater surface. The bentonite samples were initially exposed to dry N₂ heated (10°C/min) to 100°C holding this temperature for 30 minutes. Still under dry N₂, the temperature was increased (10°C/min) to 150°C for another 30 minutes. Subsequently, the temperature was decreased to 60°C for 60 minutes to the expose the bentonite to a succession of dry and humid cycles (60 % RH in the generator; 50% RH close to the sample) using flowing water-wet and dry N₂ atmospheres to hydrate and dehydrate the samples. Cyclical hydration/dehydration provides information about the adsorption/desorption rates of water, quantity of water adsorbed, and energetics of hydration/dehydration reaction. It should be noted that these TGA/DSC thermal analyses were conducted in a different manner to those described in Jové Colón et al. (2018). The latter were mainly a standard characterization of the bulk bentonite thermal properties from 20 – 1100 °C. Tajeddine et al. (2015) and Vieillard et al. (2016) conducted TGA/DSC studies on MX-80 montmorillonite (Na-dominant). Villar et al. (2017) performed TGA/DSC on FEBEX-DP bentonite from other sampled sections. Overall, the TGA/DSC profile up to high temperatures of Villar et al. (2017) and that obtained for bulk FEBEX bentonites from Section 49 are generally similar as shown in Jové Colón et al. (2018). To the knowledge of the authors, with exception of the results reported in Jové Colón et al. (2019), no cyclical hydration/dehydration TGA/DSC study on bentonite has been conducted under controlled RH and temperature conditions. The advantage of this approach is that allows for accurate kinetic studies of water adsorption/desorption cycles for given interval durations at constant RH under controlled isothermal conditions. It also allows for characterizing the effects of thermal treatment on bentonite water adsorption/desorption.

Fig. 4a shows a representative temporal TGA/DSC profile of water adsorption/desorption cycles at 60°C as a function of time (minutes) for sample BG-C-49-3 away from the heater surface. The green line in this graph shows the water adsorption/desorption cycles with the upper plateau (hydration) and the appearance of a second peak or a “dehydration shoulder” during the dehydration path. The first hydration cycle time interval is denoted by the horizontal bracket in black. The dehydration time interval from the onset of dehydration to the appearance of the second peak or “dehydration shoulder” is shown by the red horizontal (inverted) bracket. Notice that this second peak or “dehydration shoulder” is present in all the hydration/dehydration cycles. The appearance of the second peak during dehydration is hypothesized as the effect of strongly-bonded water, possibly the first water layer (1W), in the swelling smectite clay basal interlayer region (see Section IV of this report). A closer look to the hydration plateau data shows that it's not entirely flat suggesting very small sample weight gains with hydration. However, these weight gains are rather small and the trend appears to be reaching steady-state within the time interval. Similarly, after the second peak or “dehydration shoulder” the sample keeps decreasing in weight or losing H₂O but at a much slower rate even under dry conditions. These observations indicate the effects of interlayer cation hydration on adsorption/desorption kinetics therefore affecting water transport during clay hydration/dehydration. Fig. 4b shows the DSC measurements as a function of elapsed time for the dehydration interval to outline the shifts in the second peak or “dehydration shoulder” for hydration time durations of 60 and 180 minutes. A plot of the time intervals for the sample hydration, and the time interval between the onset of dehydration (t_0 in Fig. 4a) to the second peak shows a good linear correlation shown in Fig. 5. We are still assessing the significance of this correlation between hydration duration and the time interval for the appearance of the second peak during dehydration. Based on these data, the new TGA/DSC experiments in this report were conducted to mainly evaluate the potential effect of grain size and duration of the hydration cycle for the FEBEX

bentonite sample on the cyclical hydration/dehydration profiles. Bentonite samples with less than 2 μm grain size are considered of higher relative to the bulk bentonite samples shown in Fig. 4.

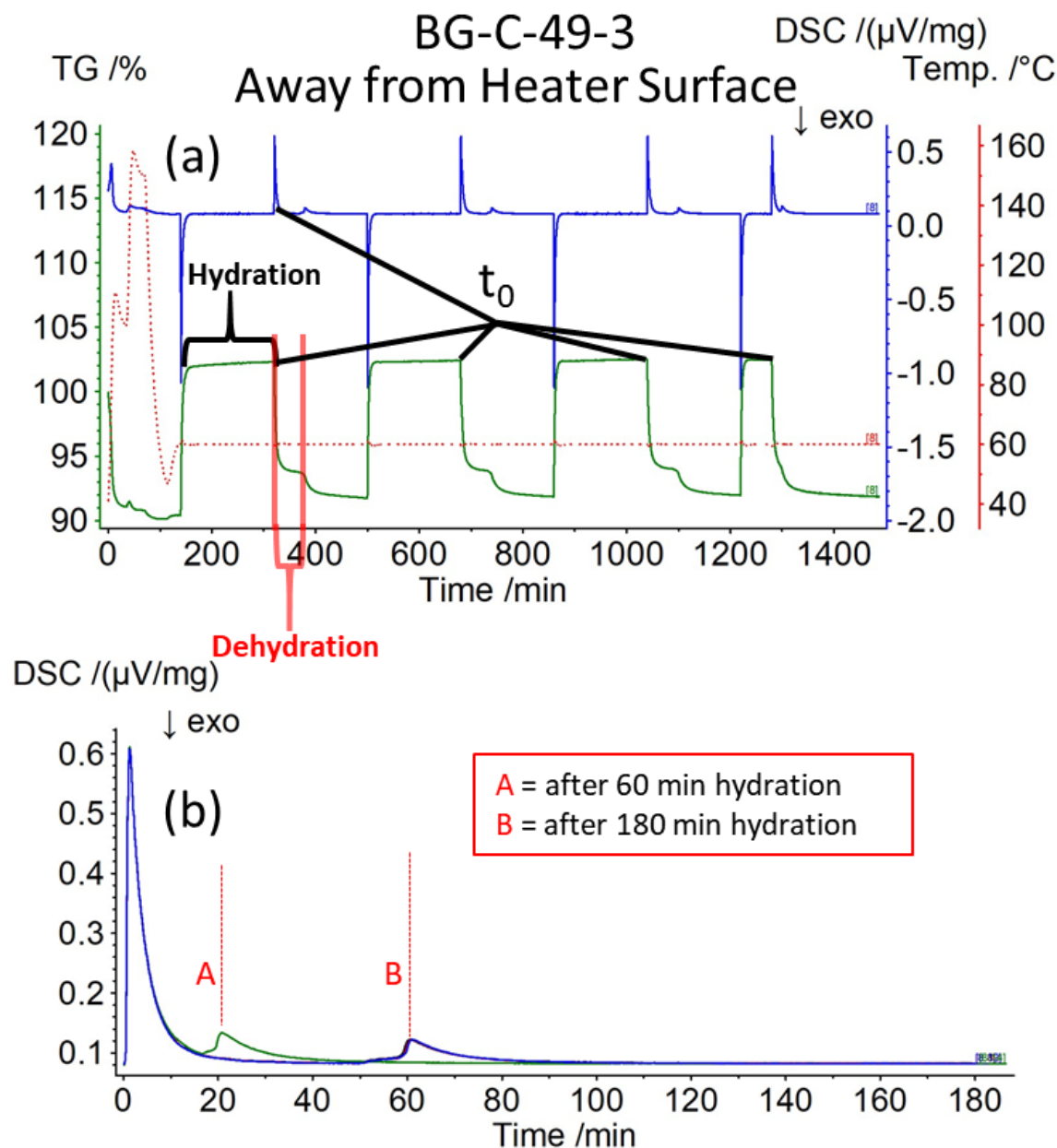


Figure 4. TGA/DSC curves as a function of time (minutes) for water adsorption/desorption cycles at 60°C for sample BG-C-49-3 away from the heater surface. (a) The green curve represents the thermogravimetric analysis (left y-axis). The blue curve stands for the DSC analysis (right y-axis). The red dotted line signifies the temperature (2nd right y-axis). The first hydration time interval is denoted by the horizontal bracket in black. The dehydration time interval from the onset of dehydration to the appearance of the second peak or "dehydration shoulder" is shown by the red horizontal (inverted) bracket (see text). (b) DSC measurements as a function of elapsed time for the dehydration interval showing the shifts in the second peak or "dehydration shoulder" for hydration time durations of 60 and 180 minutes. The starting time for dehydration (or t_0) corresponds to the onset of dehydration designated by t_0 in graph (a) at each hydration/dehydration cycle. Curves for 180 minutes hydration (B) cycles overlap and are not differentiated within the time scale of the diagram.

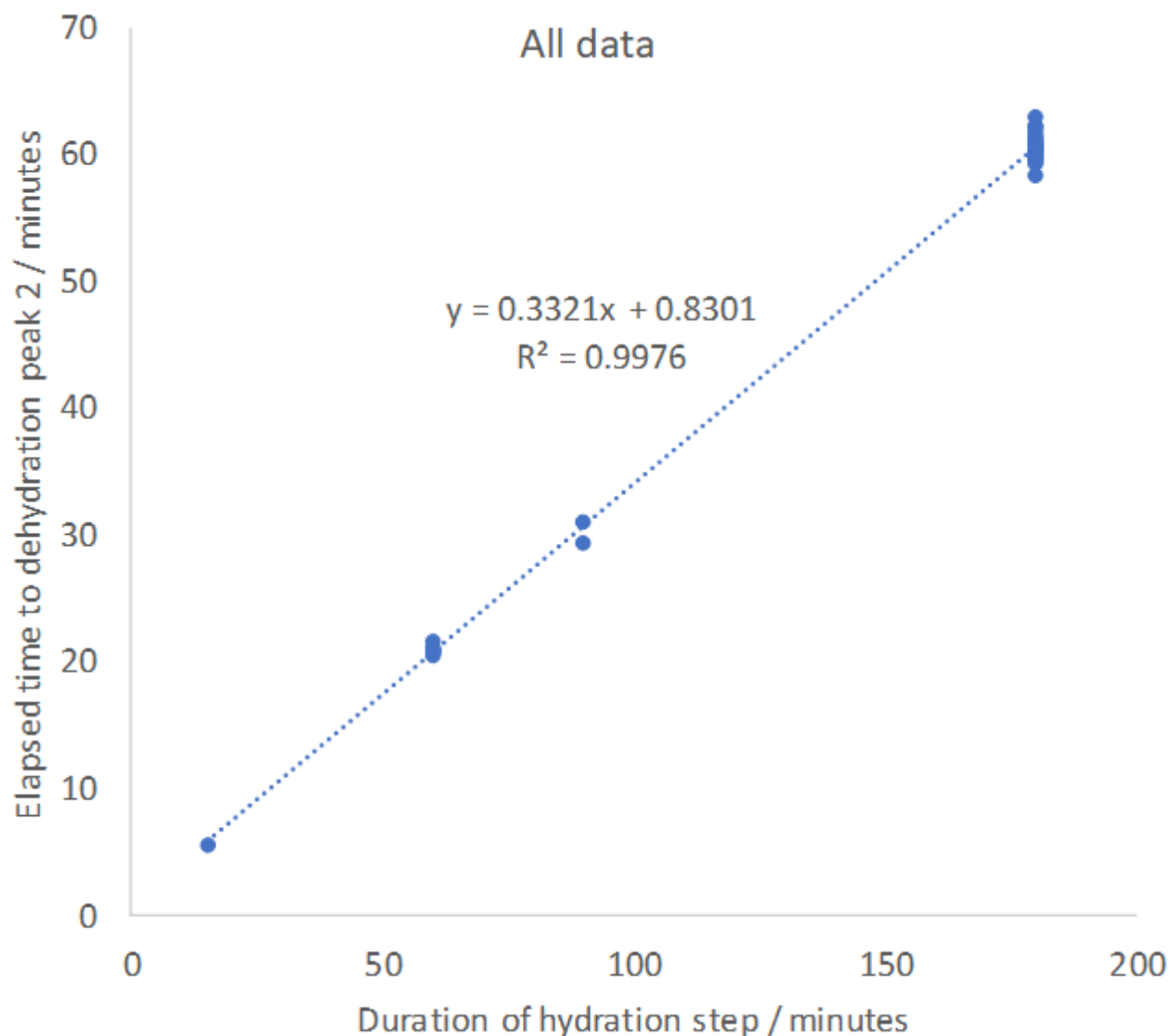


Figure 5. Elapsed time for dehydration for the appearance of the second peak as a function of hydration duration in cyclical TGA/DSC studies of water adsorption/desorption. The plot shows data for all analyzed FEBEX-DP samples.

Fig. 6a shows a representative temporal TGA/DSC profile of water adsorption/desorption cycles at 60°C as a function of time (minutes) for the less than 2 μm sample. Similar to Fig. 4a, the green line in this graph depicts the mass of the sample as it responds to changing RH during water adsorption/desorption cycles. Panels b and c of Fig. 6 depict the desorption steps only, represented by TGA and differential TGA (or DTA) in panel b, and DSC in panel c. Notice that the x-axes in these panels refers to dehydration time. The data in these plots show that the dehydration behavior is clearly a function of the duration of hydration that precedes it. Short duration hydration steps (i.e., less than two hours; curves A-D in Fig. 6) result in a dehydration process that is almost complete relative to the “dry” baseline of these cycles within a time span of approximately 45 minutes after switching back to dry gas. This is represented by a single dehydration peak in both DTA and DSC plots. As the duration of the hydration step increases beyond two hours (curves E-G in Fig. 6), however, the subsequent dehydration takes a more complex form, with a changing slope in the TGA curve and clearly shown as negative peaks in the DTA plots. Note that these show up as endotherms in the DSC plots and do not begin at the onset of the bentonite dehydration, but some time thereafter.

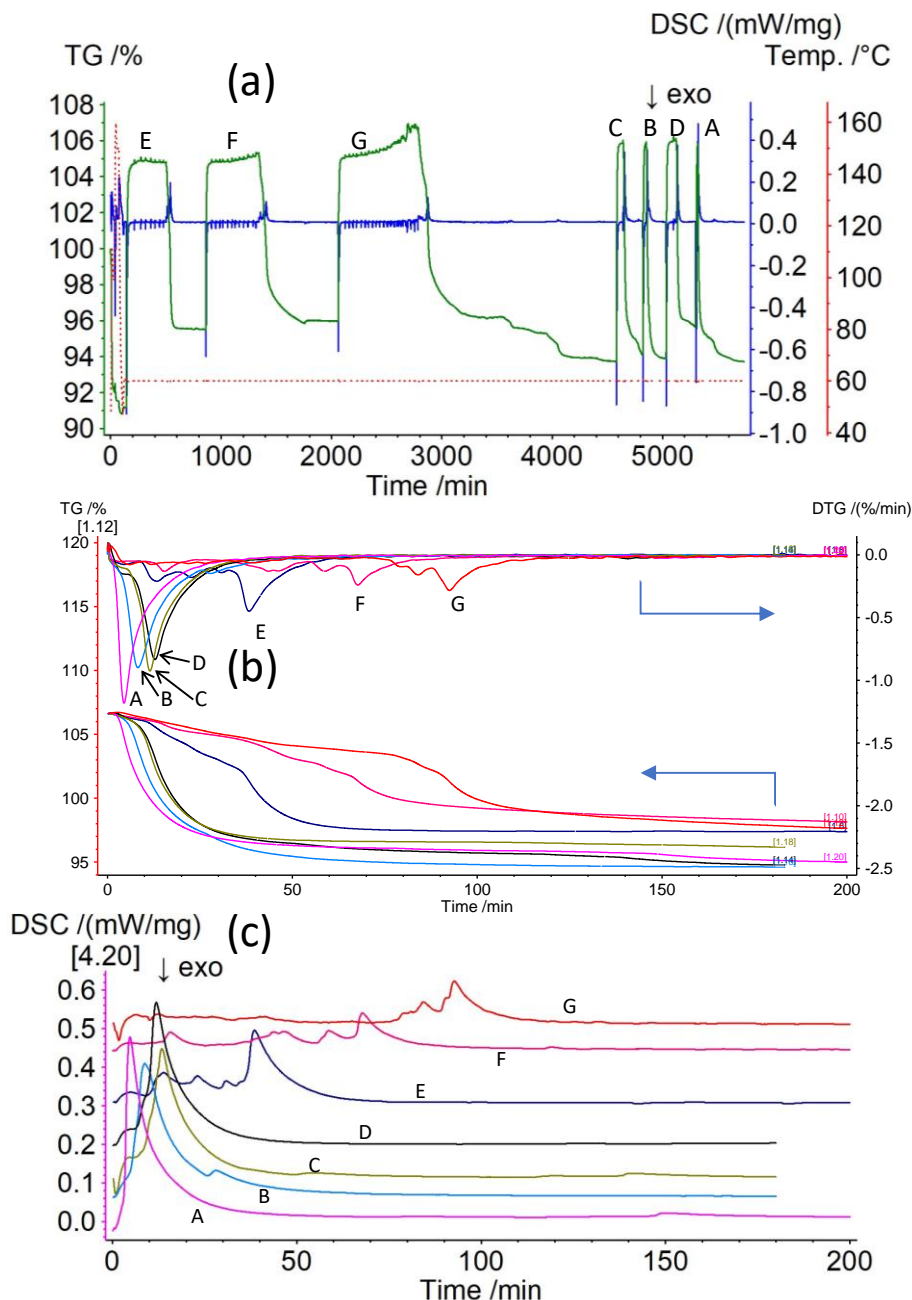


Figure 6. TGA, DTA, and DSC curves as a function of time for water adsorption/desorption cycles at 60°C for the 2 μm bentonite sample. (a) The green curve represents the thermogravimetric analysis (left y-axis). The blue curve stands for the DSC analysis (right y-axis). The red dotted line signifies the temperature (2nd right y-axis). The period of hydration was varied for each cycle, as depicted by the curve labels; A = 15 min, B = 30 min, C = 1 hour, D = 1.5 hours, E = 6 hours, F = 8 hours, and G = 12 hours. (b) TGA (lower) and DTA (upper) curves for the dehydration steps only, plotted against dehydration time. Curve labels identical to panel (a). (c) DSC measurements as a function of elapsed time for the dehydration steps; curves have been offset on the y-axis for clarity.

Note that the DTA and DSC traces are essentially mirror images of each other, since any loss of mass of the sample (DTA) is accompanied by a heat flow signal that is proportional (DSC). Figs. 7 and 8 present similar data recorded for the 38 μm and 75 μm bentonite samples, respectively. Similar behavior for these two larger grain sizes was observed when compared to the 2 μm sample.

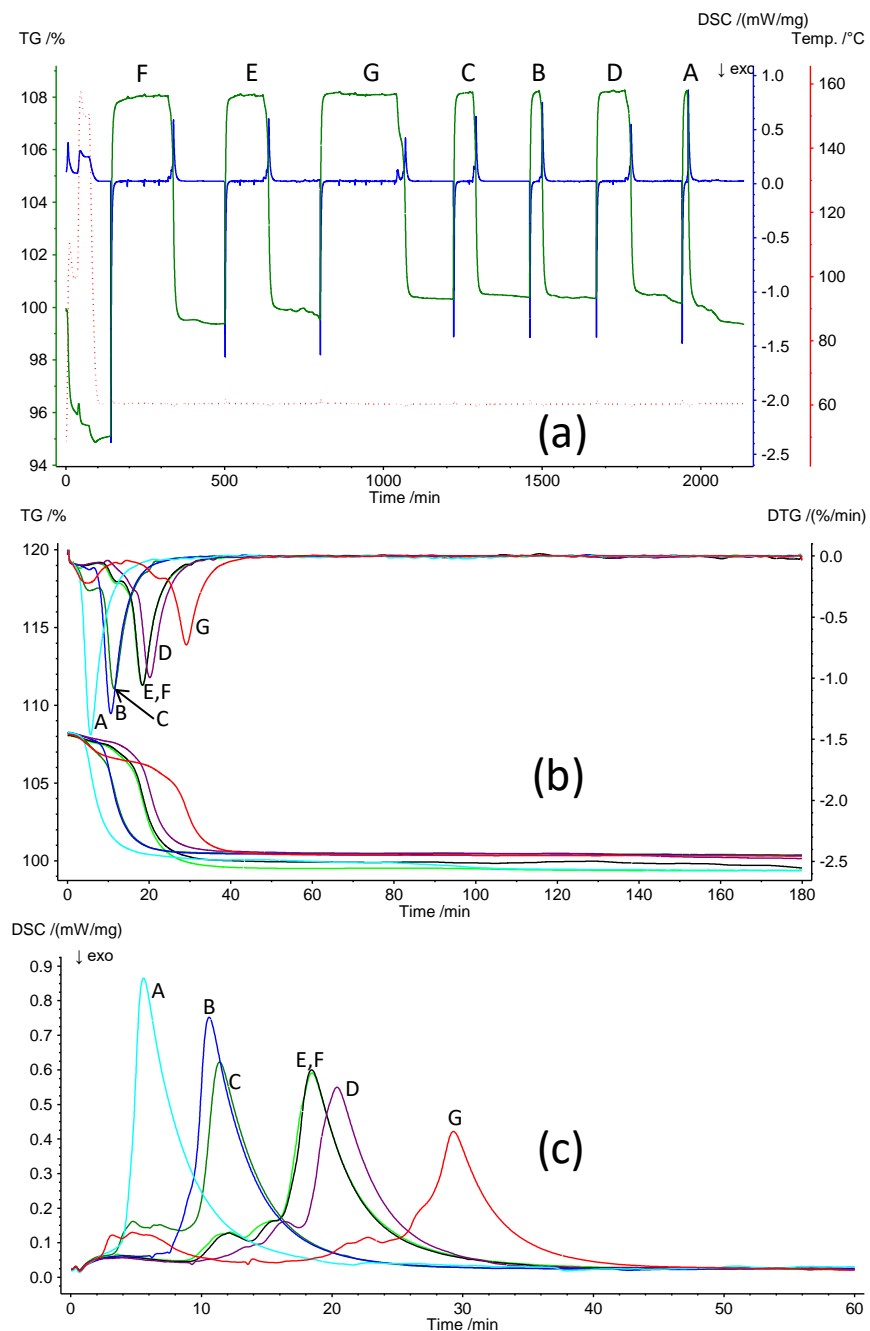


Figure 7. TGA, DTA, and DSC curves as a function of time for water adsorption/desorption cycles at 60°C for the 38 μm bentonite sample. (a) The green curve represents the thermogravimetric analysis (left y-axis). The blue curve stands for the DSC analysis (right y-axis). The red dotted line signifies the temperature (2nd right y-axis). The period of hydration was varied for each cycle, as depicted by the curve labels; A = 15 min, B = 30 min, C = 1 hour, D = 1.5 hours, E = 2 hours, F = 3 hours, and G = 4 hours. (b) TGA (lower) and DTA (upper) curves for the dehydration steps only, plotted against dehydration time. Curve labels identical to panel (a). (c) DSC measurements as a function of elapsed time for the dehydration steps; first 60 minutes only.

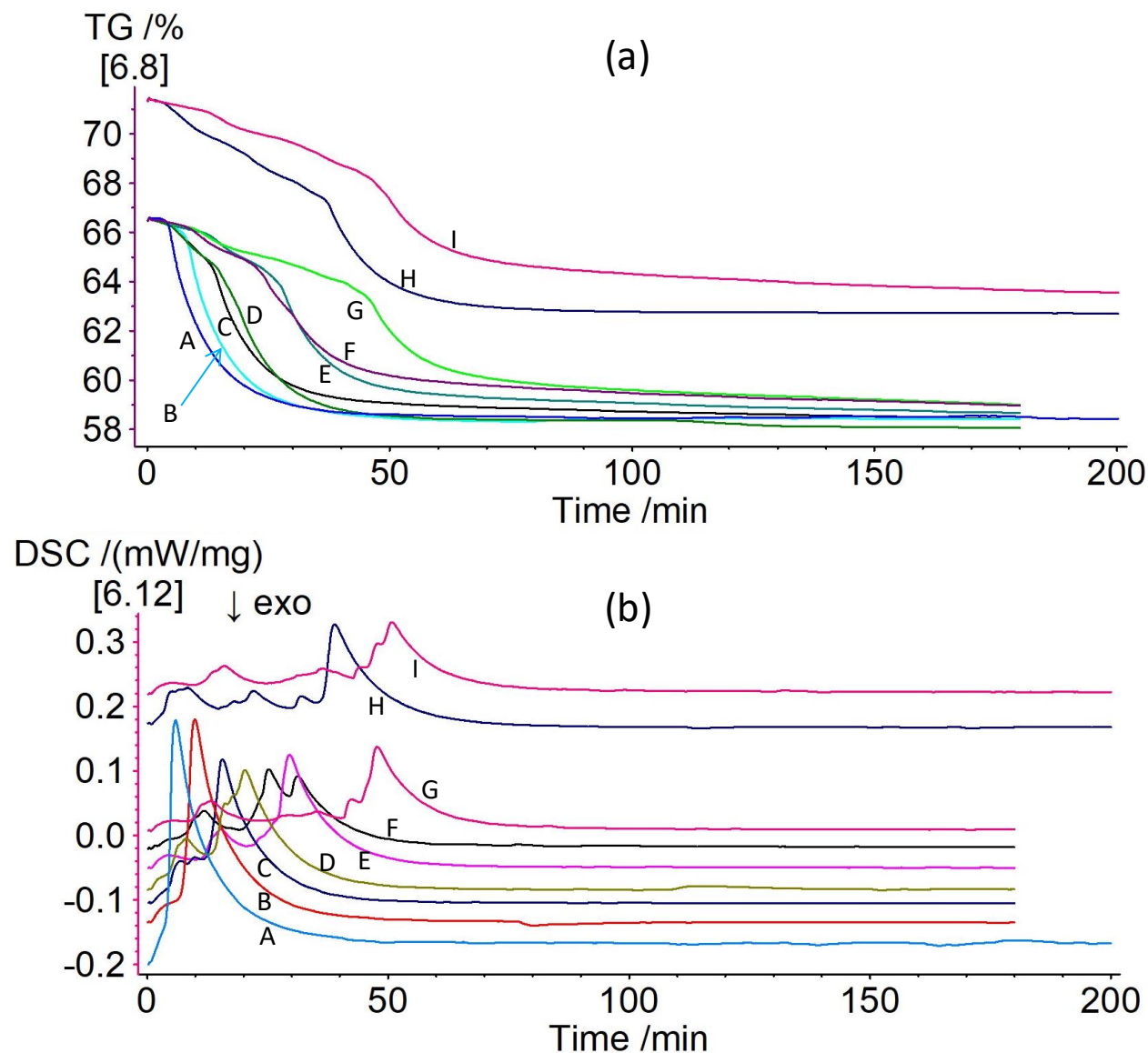


Figure 8. TGA and DSC curves as a function of time for water adsorption/desorption cycles at 60°C for the 75 μm bentonite sample. (a) TGA curves for the dehydration steps only, plotted against dehydration time. The period of hydration was varied for each cycle, as depicted by the curve labels; A = 15 min, B = 30 min, C = 1 hour, D = 1.5 hours, E = 2 hours, F = 3 hours, G = 4 hours, H = 6 hours, and I = 8 hours. (b) DSC measurements as a function of elapsed time for the dehydration steps; curves have been offset on y-axis for clarity. Curve labels identical to panel (a).

The TGA/DSC studies by Tajeddine et al. (2015) and Vieillard et al. (2016) on MX-80 bentonite were conducted on samples equilibrated at different RH's. These authors also described the differences in water adsorption/desorption in terms of the energetics of these two processes in the montmorillonite clay. They observed that at high RH, the retrieved standard enthalpies of formation for sorbed water resemble those of liquid water whereas at low RH it suggests strong adsorption of the first water monolayer (Tajeddine et al., 2015). These results are consistent with those obtained in the current cyclical TGA/DSC thermal study of FEBEX-DP bentonite hydration/dehydration where differences in the rates of water adsorption/desorption indicate different mechanism for these two processes. This is suggested by the reproducible and recurring appearance of a second peak or “dehydration shoulder” during the dehydration leg indicating the presence of strongly-confined

water, most likely in the form of a one-layer (1W) hydrate in the smectite interlayer region. Teich-McGoldrick et al. (2015) conducted molecular simulations to describe the swelling properties of montmorillonite clays of various cationic compositions and their hydration modes during water uptake. There are some parallels between the molecular modeling and the current experimental work suggesting the predominance of a one-layer (1W) hydration mode in the clay interlayer at low RH during dehydration. Bish and Carey (2001) describe the thermal behavior of zeolites in response to RH suggesting the existence of energetically distinct types of water in the mineral structure. Fridriksson et al. (2003) observed changes in the crystal structure of laumontite zeolite in response to hydration/dehydration conditions suggesting various levels of water occupancy at distinct sites. The structural differences between zeolites and layered silicates such as smectite clay makes the analogy of distinct water sites not entirely applicable except for generalizing the potential existence of weakly- and strongly-confined waters on the clay surface and interlayer region. These thermal analyses could shed light in describing the typical hysteretic behavior of swelling smectite clays during water adsorption/desorption. Another salient feature of these analyses is that there were no significant differences in the temporal TGA/DSC profiles of hydration/dehydration cycles for all bentonite samples at locations close and far from the heater surface. Although there were some differences in the maximum extent of swelling for bentonite samples locate close to the heater surface Jové Colón et al. (2018, 2019), these were relatively small compared to those farther from the heater surface. More experimental work is needed to address the nature of hydration modes in swelling clay and the relation to structural changes in response to hydration/dehydration cycles. Section IV is an attempt to utilize molecular dynamics (MD) simulation to assess the mechanisms of water behavior in the smectite interlayer during evaporation. Work is planned to conduct cyclical TGA/DSC with variation in hydration/dehydration time durations at slightly higher temperatures. There are also plans for exploratory XRD studies under controlled RH and temperature to complement the cyclical TGA/DSC experiments. An important aspect of these thermal studies to assess the impact of temperature on bentonite swelling and water uptake given the anticipated high thermal loads from large canisters (e.g., dual purpose canisters or DPC's) on the surrounding bentonite barrier.

IV. Water transport mechanism in clay interlayer during the dehydration

Motivated by the results obtained in the TGA/DSC study described in the previous section, molecular dynamics (MD) simulations were conducted using the LAMMPS simulator (Plimpton, 1995) to study water transport mechanisms in the interlayer of Na-Montmorillonite (Na-MMT) along with the structural transformation of hydrated Na-MMT during the dehydration process. Fig. 9 represents the MD simulation box ($150 \times 31.06 \times 200 \text{ \AA}^3$) containing a Na-MMT particle with 10 interlayers where each one accommodates 2 hydration layers (2W). The Na-MMT particle has 2 edges facing the vacuum region. When applying periodic boundary conditions for all directions, the particle become infinite in the x and y directions and finite ($\sim 110 \text{ \AA}$) in the z direction.

During the dehydration simulations, water molecules that move to the vacuum space (i.e., between the dash line and the boundary of the simulation box) are remove at a constant rate of 5 water molecules per picosecond (i.e., $5w/ps$). The simulation box can change (e.g., shrink) in the x direction according to the pressure of 1 atm. The simulations were conducted at a temperature of 300 K.

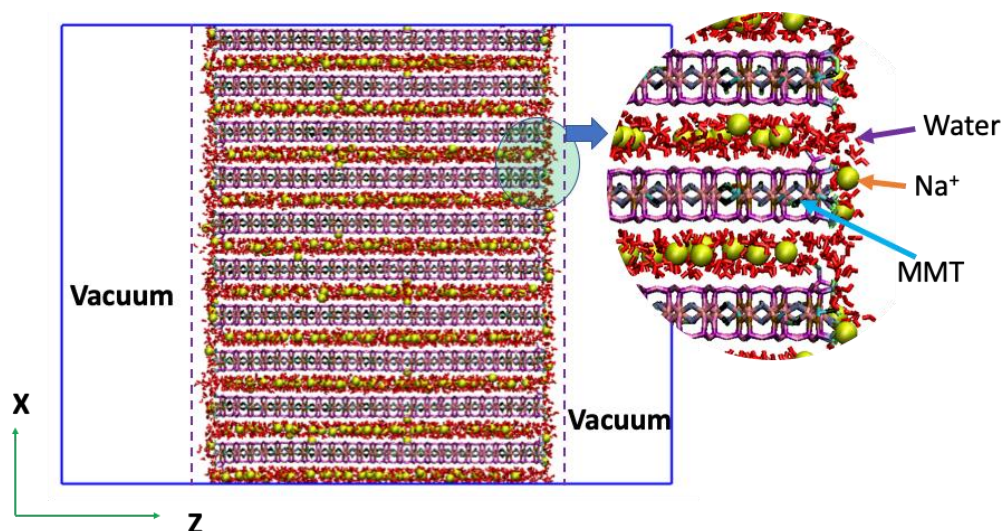


Figure 9. Simulation system used to study the dehydration process of Na-Montmorillonite. Red sticks represent water molecules, the green balls symbolize the Na^+ atoms, and the purple framework structure stands for the Na montmorillonite. The inset circle denotes the clay edge region enlargement at right.

In Fig. 10 we report the number of atoms in the simulation box as a function of simulation time during the dehydration simulation (number of atoms decreases because of water removal as discussed above). At the beginning of the simulation, there are two hydration layers in each interlayer (see point A in top left panel of Fig. 10, and snapshot A). As dehydration progresses, the number of atoms linearly decreases to point B. The B snapshot indicates that at point B, there is one hydration layer in each interlayer (1W). Further dehydration decreases the number of atoms in the system in a nonlinear manner. At point C, there is a small number of water molecules in the interlayer (see snapshot C).

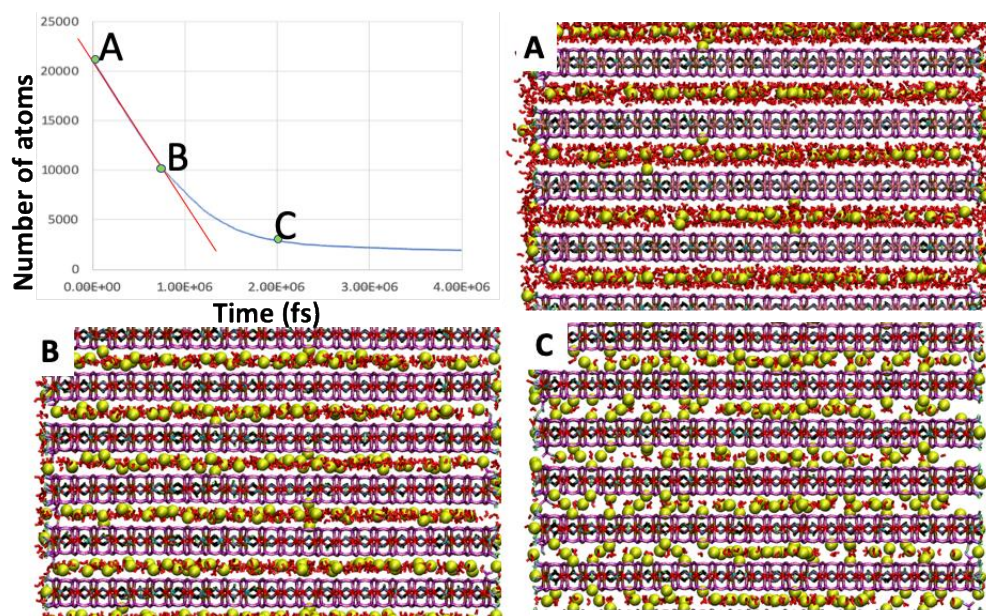


Figure 10. Number of atoms in the MD simulation box as a function of time (top left panel). Snapshots labeled A, B, and C are the configurations for the points A, B, and C marked in the top left panel. These snapshots represent the structural transformation of the Na-MMT during dehydration process. The red line in the top left panel demonstrates the linear dehydration process.

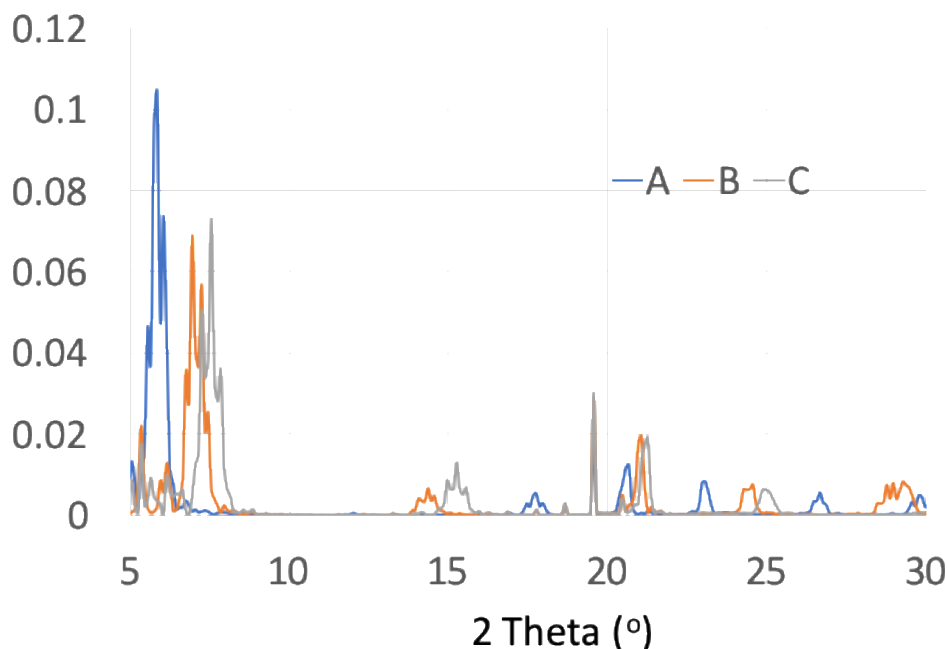


Figure 11. Calculated XRD pattern for the Na-MMT structures reported in snapshots A, B, and C shown in Figure 10.

Experiments on FEBEX bentonite involving characterization of clay structural changes monitored as a function of RH and temperature using an *in-situ* XRD technique are planned. MD simulations of the hydrated Na-MMT structure during the dehydration process can be used to generate XRD spectra of the different hydration states. Fig. 11 shows the calculated XRD spectra and peak shifts for the configurations presented from MD simulation results in Fig. 10 (snapshots A, B, and C).

In the future, we plan to study the water transport mechanism at different evaporation rates (i.e., water removal rates) other than In the current report, we remove 5w/ps. We will test 3w/ps and 10w/ps. We also plan to carefully examine the water structure in the interlayer during the dehydration process. Our hypothesis is that water molecules that do not coordinate with Na^+ ions will move quickly towards the edge and are then being removed first. As we discussed in a separate manuscript by Ho, Wang, Jové-Colón, and Coker (submitted), the linear dehydration behavior presented in Fig. 10 is due to the advection of water in the interlayer. Water molecules that coordinate with Na^+ ions will be removed at a much slower rate (e.g., diffusion process) leading to a non-linear dehydration process (segment B-C) in Fig. 10. This non-linear removal of water could be related to the observed dehydration part of the thermal analysis profiles shown in Fig. 6a where water is removed at a slower rate.

V. FEBEX Bentonite Interactions with FeCl_2 Solution

Interfacial interactions between steel canister materials and expansive clay (bentonite) in the presence of an aqueous phase can influence the stability of clay in the disposal environment. Previous studies (Cheshire et al. 2018) described Fe-saponite and sulfide growth in hydrothermal experiments using Wyoming bentonite and carbon/stainless steel coupons indicating highly reduced environments at the clay/metal interface. Given the potential issue of clay stability at barrier interfaces exposed to high thermal loads in the presence of Fe, controlled atmosphere experiments using FeCl_2 (ferrous Fe) solution were performed under ambient and elevated temperatures to investigate changes in the clay phase and reacting solution.

Experimental Procedure

Two sets of experiments involving the addition of FeCl_2 solution to FEBEX bentonite samples were prepared using controlled atmospheric conditions. Experiment 1 consisted of “soaking” the samples in either water or 1 M FeCl_2 solution at room temperature in centrifuge tubes. Experiment 2 included heating the sample with these solutions in Parr[®] vessels at 200°C.

Experiment 1 (“Soaked”): XRD and ICP-OES Analyses

Experiment 1 (“Soaked”): These experiments were conducted in a nitrogen rich glovebox to prevent oxidation. Three sample designations were chosen for this experiment; baseline FEBEX bentonite material, B – away from heater, and BM – close to heater. 0.1 gram of each sample clay were added to 50 milliliter centrifuge tubes. Two control samples that didn’t include the FEBEX bentonite were prepared as well. Solutions of 1 M FeCl_2 were prepared by measuring the FeCl_2 salt outside the glove box but mixing the solid with deoxygenated water in the glove box. Deoxygenated water was prepared by boiling DI water (18 M Ω) for an hour then purging with nitrogen gas until cooling to ambient temperature. 8.88 milliliters of either DI or 1M FeCl_2 were added to the FEBEX samples yielding a 1:100 solid to solution ratio. The initial pH was measured on the reactors.

Table1- Experiment 1 set up of various reactors and pH data before and after soaking.

Sample ID	Mass of Sample (g)	Initial pH	Final pH
Baseline- H ₂ O	0.1002	9.07	8.69
Baseline- FeCl ₂	0.1004	2.24	2.31
B away- H ₂ O	0.1001	8.36	8.05
B away- FeCl ₂	0.1005	2.17	2.23
BM close- H ₂ O	0.0997	7.91	7.55
BM close- FeCl ₂	0.0999	2.19	2.23
Control- H ₂ O	N/A	5.97	4.64
Control- FeCl ₂	N/A	2.07	2.08

The samples were left in the glove box to soak and mixed using a rotating shaker for 48 hours. After the 48 hours period, the pH was measured before sampling. The samples were transferred out of the glovebox for centrifugation. Once centrifugation was completed, the samples went back into the glovebox to open reactor tubes, collected supernatant, filtered using 0.2 μm syringe filters, and transferred to new centrifuge tubes for liquid analysis. The clay pellets that remained were then rinsed with deoxygenated water; 10 milliliters of water were added and allowed to shake for an hour. Then these were centrifuged, and water supernatant was filtered and collected for liquid analysis. The liquid samples were acidified using concentrated nitric acid (for every 1 mL of solution, 10 μL of acid was added). The remaining rinsed clay pellets were allowed to dry in the nitrogen glovebox, to prevent oxidation. Unfortunately, the glovebox turned oxic while the “soaked” samples were drying. It should be noted that the glove box was anoxic during the experiment. This oxic event caused the development of a rust ring formed at the top of the samples, before the samples were fully dry. The presumably oxidized dark orange portion of the pellet was separated from the normal clay colored (tan) sample and was analyzed using X-ray diffraction (XRD). The XRD spectra obtained for these experiments are shown in Fig. 12. The oxidized portion of the baseline sample as shown in Fig. 12(a) show a shift in the (001) peak (left peaks at low 2θ angle) of the oxidized sample towards a larger 2θ value and smaller $d(001)$ spacing relative to those under reduced conditions.

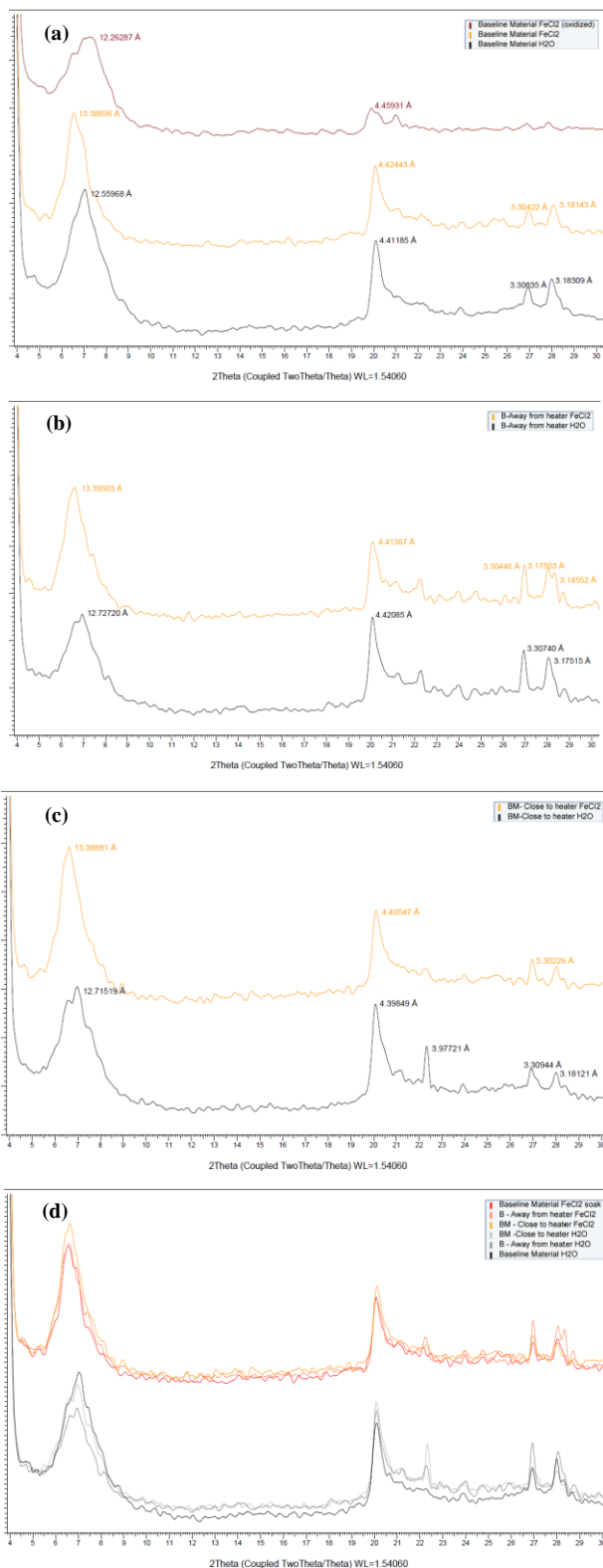


Figure 12: XRD spectra of “Soaked” experiments comparing samples soaked in FeCl₂ and H₂O along with d-spacing values (a, b, c) for major peaks. Panels (a), (b), and (c), show XRD spectra of “Soaked” experiments for baseline sample, B (away from heater), and sample BM close to heater, respectively. Panel (d) shows a stacked spectra summary plot of the various materials and their soaking solutions.

The reacted supernatant and rinsed solution were saved and analyzed using ICP-OES. Each sample was diluted by a factor of 1:100 using 2% optima nitric acid. These were analyzed using a Perkin Elmer Optima 8000 Inductively Coupled Plasma – Optical Emission Spectrometry (ICP-OES) to obtain total solution concentrations of iron, silica, magnesium, calcium, aluminum, sodium, and potassium. For iron measurements, samples were diluted 1:10,000 since the iron concentration was initially too high (1M or 55,844.77 ppm) and could saturate the detector. The results for the various elements are shown in Figs. 13 and 14.

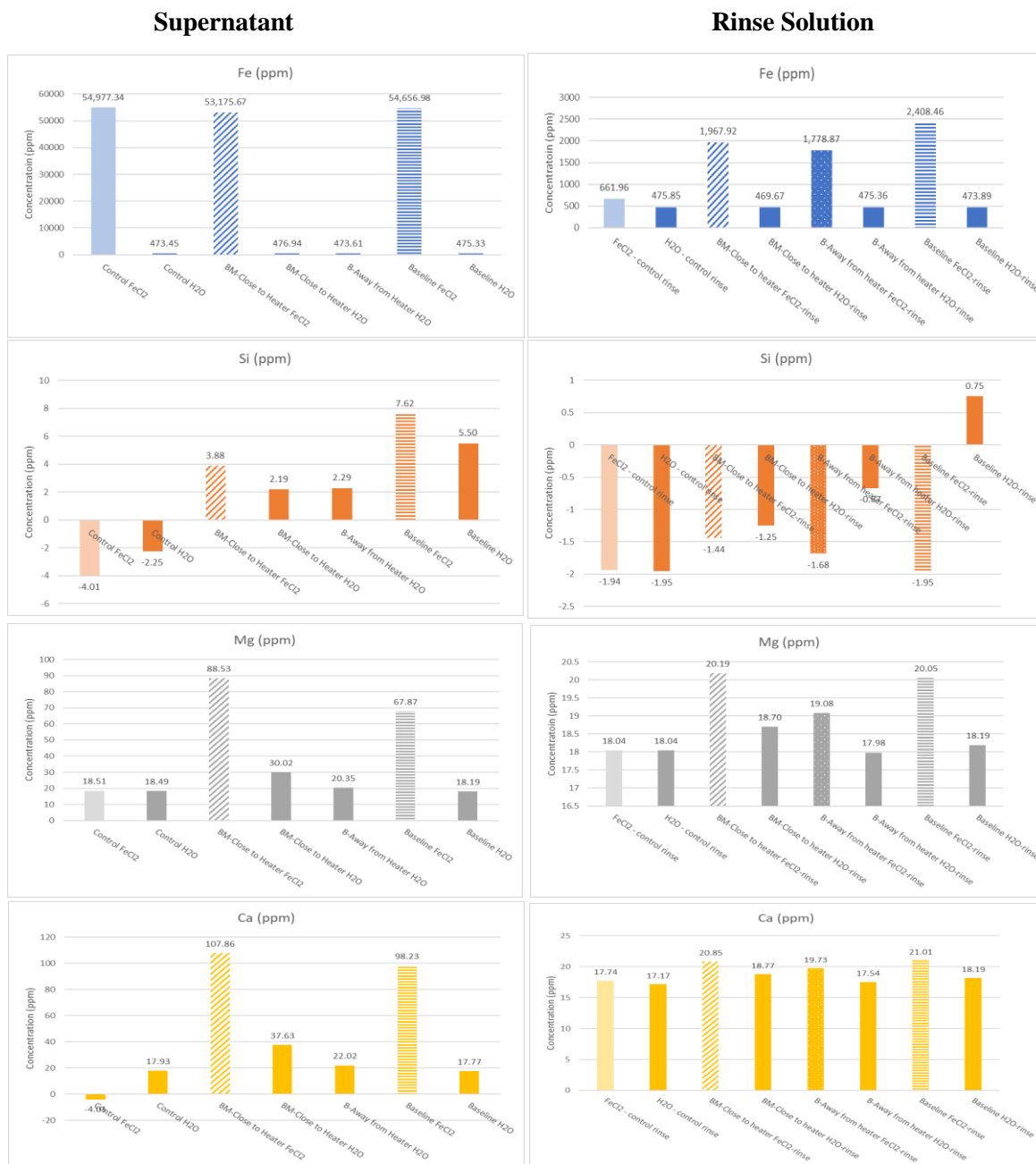


Figure 13. Fe, Si, Mg, and Ca concentrations in supernatant and rinse solutions for “Soaked” experiments. The panels on the left show element concentrations of the reacted supernatant whereas on the right show the rinse solutions. Negative concentrations signify either below detection or not detected.

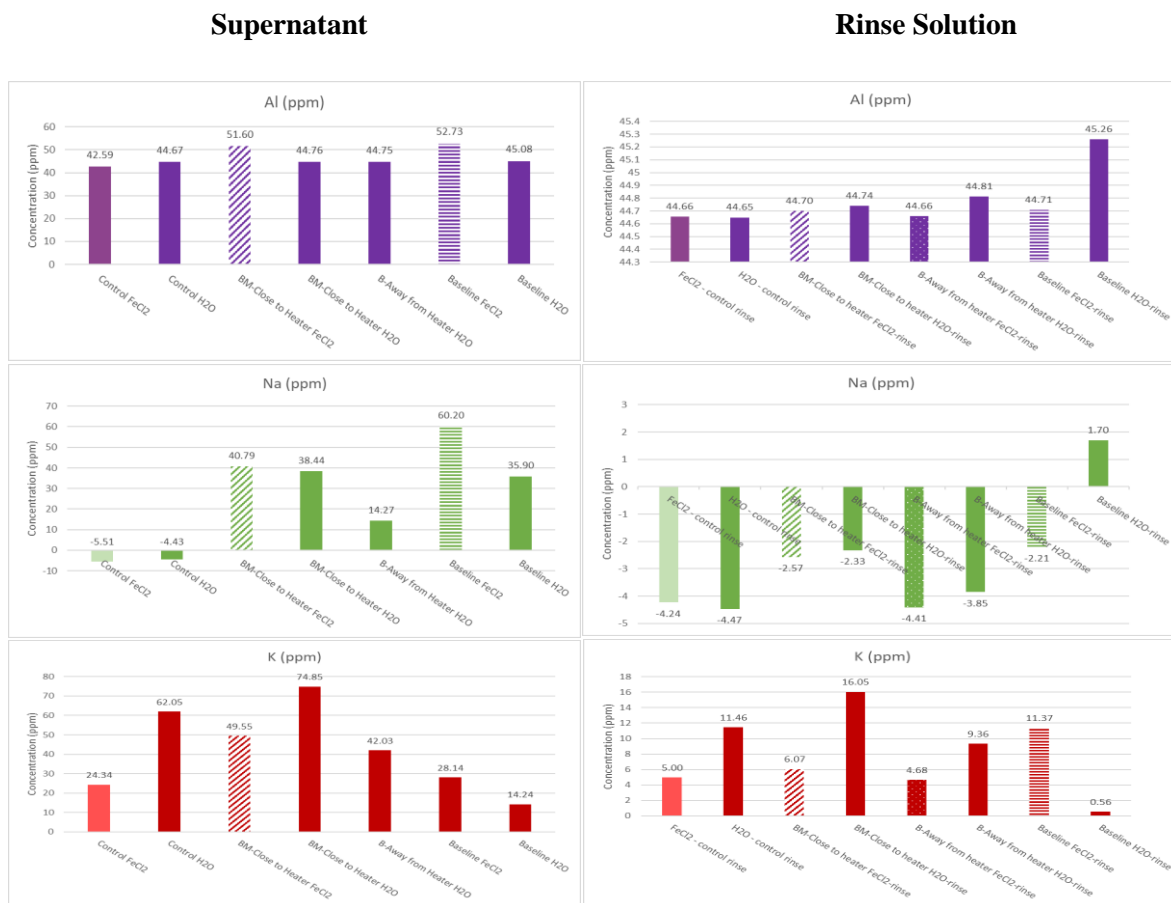


Figure 14. Al, Na, and K concentrations in supernatant and rinse solutions for the “Soaked” experiments. The panels on the left show element concentrations of the reacted supernatant whereas on the right show the rinse solutions. Negative concentrations refer to either below detection or not detected.

Experiment 2 (Heated): XRD and ICP-OES Analyses

Parr[®] vessels were used to conduct heated experiments with clay samples and solutions. Samples were composed of baseline and BM (close to heater) FEBEX bentonite material. 1.69 grams of each sample was measured and added to the Parr[®] vessel Teflon cups (4 samples total). 1M FeCl₂ was prepared in the same manner as in Experiment 1 with all materials transferred to the glove box. 150 mL (1:100 solid to solution ratio) of either DI-deoxygenated water or 1M FeCl₂ was added to their respective Teflon cups. Initial pH was collected in all samples.

Table 2- Experiment 2 set up of various reactors and pH data before and after heating.

Sample ID	Mass of Sample (g)	Initial pH	Final pH	Mass after (g)
Baseline- H ₂ O	1.6898	9.40	8.10	1.5322
Baseline- FeCl ₂	1.6907	2.18	2.14	1.7465
BM close to heater- H ₂ O	1.6903	8.47	6.71	1.5724
BM close to heater- FeCl ₂	1.6902	2.19	1.99	1.6996

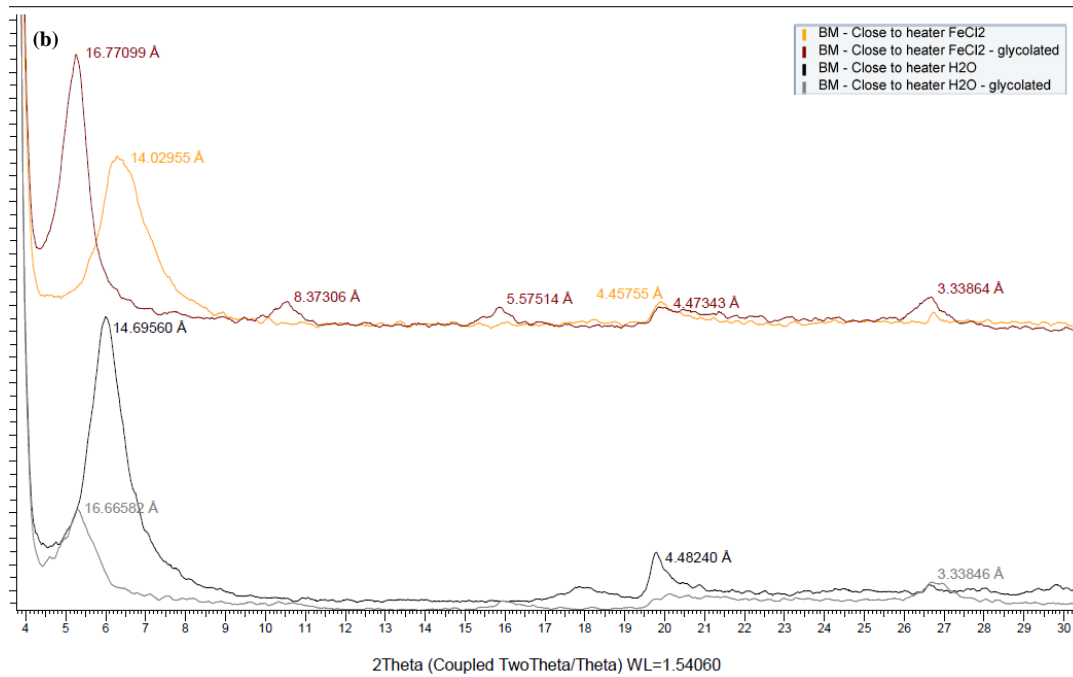
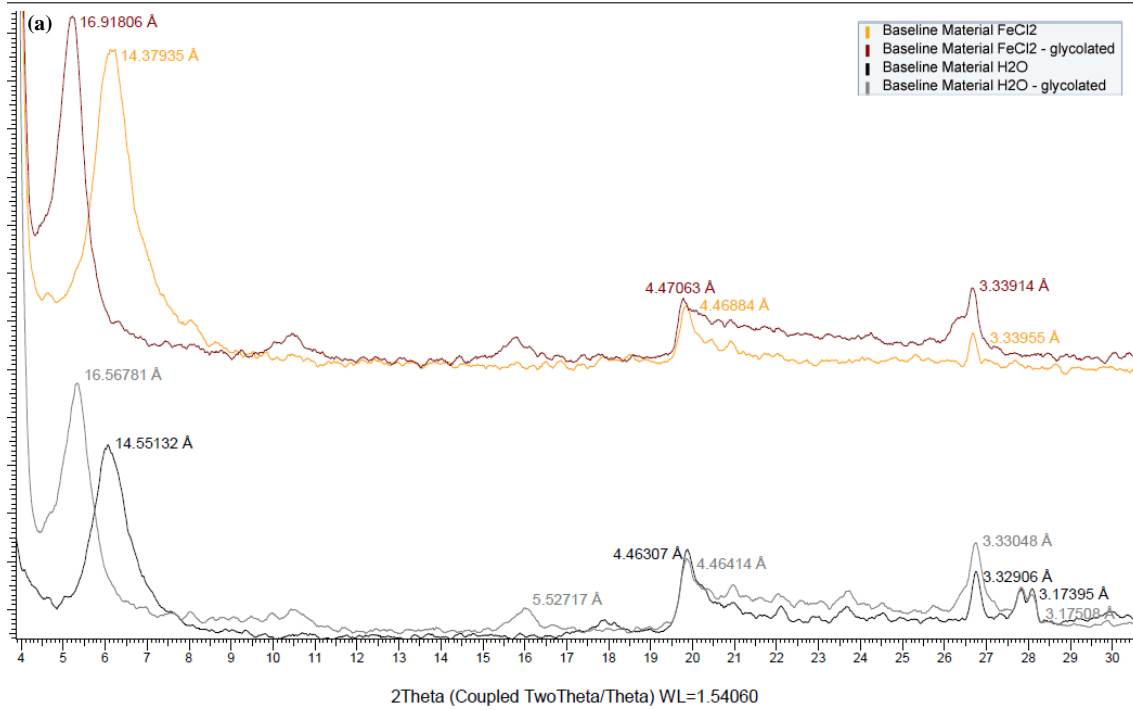


Figure 15. XRD spectra of FEBEX bentonite for Experiment 2 (Heated). Panel (a) represent Baseline material reacting in water and FeCl₂. Panels (b) refer to samples close to the FEBEX heater reacting in water and FeCl₂. Each panel shows a comparison between glycolated and non-glycolated samples.

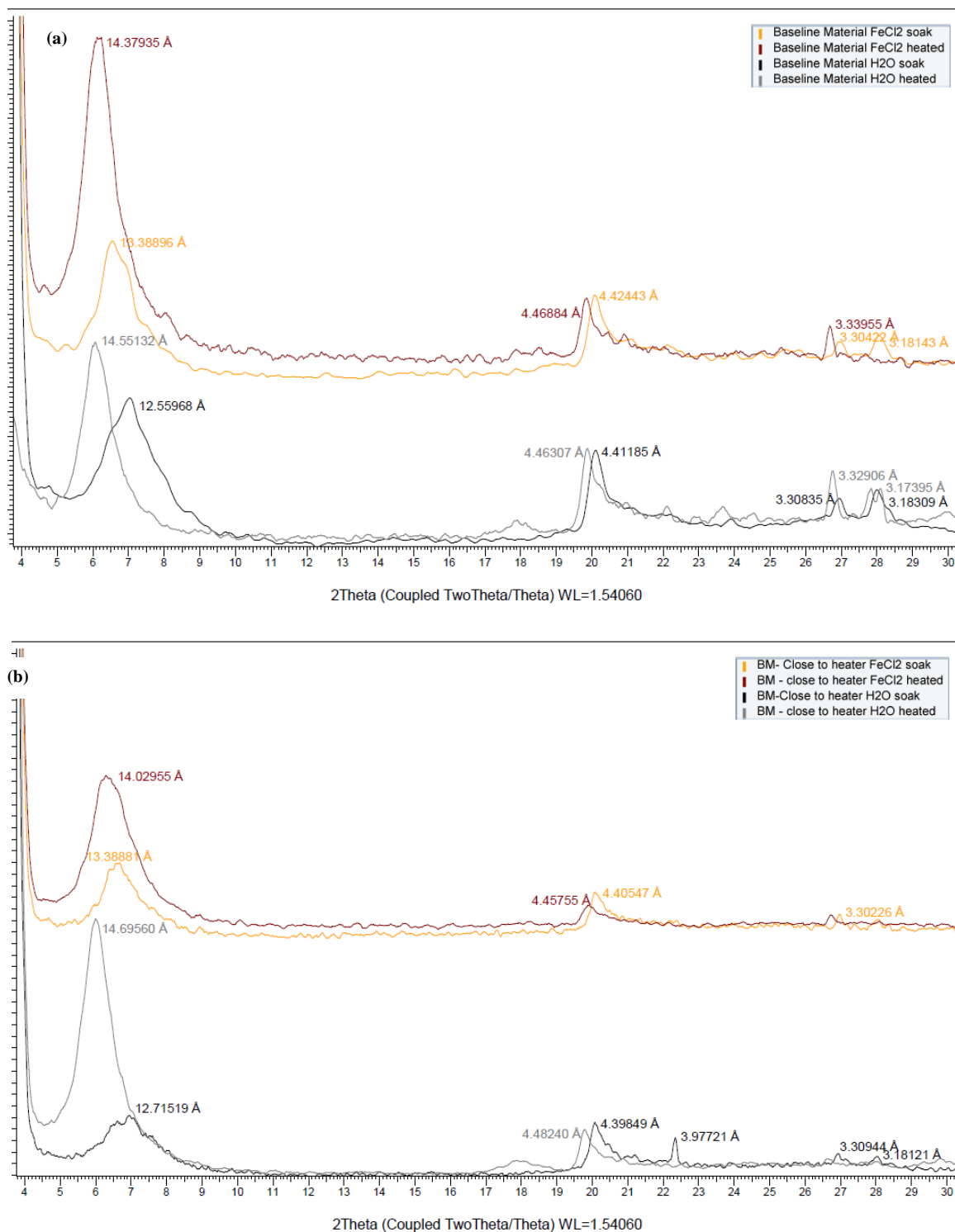


Figure 16. XRD spectra for FEBEX bentonite samples (Baseline and close to the heater). Panel (a): Comparison between soak and heated experiments for Baseline material in either water or FeCl₂. Panel (b): Comparison between soak and heated experiments for material close to the heater in either water or FeCl₂.

The Parr® vessels were assembled in the glovebox, and subsequently removed to be then placed in an oven at 200°C for seven days. After this time period, the oven was turned off and vessels were allowed to cool in the oven for 24 hours. Afterwards, the vessels were taken into the glove box to collect solid and liquid samples for subsequent analysis. The par vessels were opened inside the glove box and pH was measured immediately. Clay/solution mixtures were transferred to centrifuge bottles and removed from glove box for centrifugation. The supernatant was collected and acidified using concentrated nitric acid (10 µl concentrated HNO₃ per 1 mL of liquid). The remaining clay pellet was rinsed with 40 mL deoxygenated water and supernatant was collected (a total of 2 water rinses were performed). The clay that remained in the bottles was allowed to dry in nitrogen glove box. The reacted samples were then analyzed on the XRD. Oriented XRD mounts were prepared, and XRD analysis also included glycolation to measure swelling capability. Glycolation involved incubation of the XRD mounts at 60°C in a small desiccator that contained ethylene glycol for 24 hours. Samples were immediately removed from desiccator for XRD analysis and data collection. The XRD spectra obtained for these experiments is shown in Fig. 15. Fig. 16 shows stacked XRD spectra comparing samples from experiments in water and FeCl₂ solutions.

In the same manner as in Experiment 1, ICP-OES the samples were diluted 1:100 for analysis of Ca, Si, Al, Mg, Na, and K they were further diluted to 1:10,000 for Fe analysis; using 2% HNO₃. The ICP-OES analyses results are shown in Fig. 17.

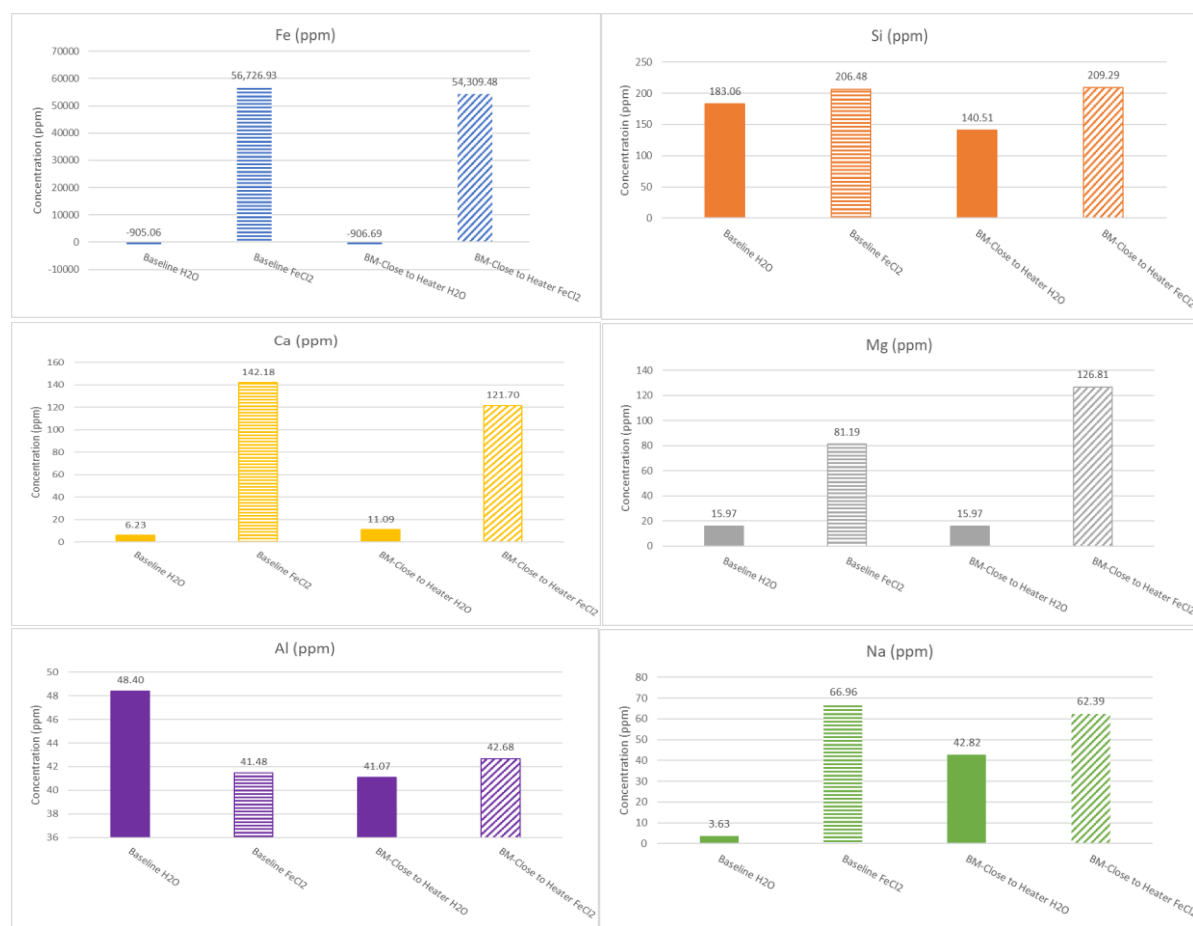


Figure 17. Fe, Si, Ca, Mg, Al, and Na concentrations for the supernatant in Experiment 2 (Heated).

Discussion

XRD analyses of “Soaked” experiments show the (001) peak shift towards lower 2θ values when the material reacted with FeCl_2 relative to the water soaked experiments (see Panel (d) of Fig. 12) resulting in larger d-spacing values. All glycolated XRD samples in Experiment 2 indicated swelling as demonstrated by a shift of the (001) reflection peak to lower 2θ values as shown in Fig. 15. Fig. 16 show that bentonite samples reacting with FeCl_2 in Experiment 2 (Heated) exhibited a marked shift in the (001) peak relative to those in the “Soaked” experiments. The (060) peak ($2\theta \approx 60\text{-}61^\circ$) yield a d-spacing of $\sim 1.49 - \sim 1.50 \text{ \AA}$ suggesting that transformation to a trioctahedral clay did not occur.

ICP-OES analysis indicate that cation with a 2+ charge (Mg^{++} and Ca^{++} ; except Fe^{++}) have a relatively larger increase in their concentrations for the FeCl_2 experiments relative to those with water. This observation could be indicative of Fe^{++} in the reacting solution exchanging for Mg^{++} and/or Ca^{++} given their release into solution. However, the pH of FeCl_2 solution is acidic (pH \sim 2) which can induce dissolution of the clay phase, although relatively small silica concentrations were measured in the supernatant. The concentrations of Al^{+++} , Na^+ , and K^+ do not show clear trends compared to Mg^{++} and Ca^{++} which suggest cation exchange occurred in these experiments. For the “Soaked” samples, the rinsed solutions did show more element removal from the clay; mostly Fe, Mg, Ca, and Al. This could indicate some level of ion exchange but it would require chemical analysis of the solids to confirm this process. Further work is planned to further characterize the composition of solid run products and additional evaluation of these structural and compositional data.

VI. DECOVALEX-2019 Task C: GREET (Groundwater REcovery Experiment in Tunnel), Mizunami URL, Japan

This section describes an update to the PFLOTRAN reactive-transport model for DECOVALEX-2019 Task C described in Jové Colón et al. (2018). The DECOVALEX-2019 project phase started this year with seven tasks (A-G) targeting various issues relevant to coupled THMC processes driven experimental and URL field data. The Disposal in Argillite work package has expressed interest in the GREET (Groundwater REcovery Experiment in Tunnel, Mizunami URL, JAEA, Japan) URL project on the hydrochemical characterization of the site as part of the groundwater recovery activity from the closure test drift (CTD). The CTD is a tunnel section (46.5 m long \times 5.0 m wide \times 4.5 m high) of the URL sealed by plug and filled with groundwater. A series of boreholes allow for monitoring water pressure and chemistry during the experiment. The current study extends the work conducted on cement interactions in the flooded CTD to evaluate shotcrete liner interactions using a 3D model representation of this domain implemented in the reactive transport simulation code PFLOTRAN. Na^+ , Cl^- , Ca^{++} concentration data and pH obtained at the site will be used as a test to the model. The GREET project task leader has kindly provided web access to the geochemical and hydrological data, as it becomes available, to be reviewed by the task participants. Hydrochemical data from the DECOVALEX-19 (Task C) was either provided by the JAEA team and/or information at the GREET website (<http://www.jaea.go.jp/04/tono/miu/dataset/greet/greet.html>). DECOVALEX-19 phase ended at the end of 2019 and moving to the next phase DECOVALEX-2023.

Closure Test Drift (CTD): 3D H-C Model of Shotcrete Liner Interactions

The Closure Test Drift (CTD) is a tunnel facility (Fig. 18) at 500 meters below ground level to investigate the effects of hydrological, geomechanical, and geochemical variations during drift excavation and post-closure in fractured granitic rock. The facility is equipped with monitoring probes for water sampling, hydraulic pressure, and rock displacement. Mapping of fractures was conducted during drift excavation. The CTD tunnel is lined with Mg-bearing ordinary Portland cement (OPC) shotcrete and is sealed by using a low-heat Portland cement plug (Iwatsuki et al.,

2017). After closure, the tunnel was filled with water to study environmental changes including effects on hydrochemistry due to interactions with barrier materials such as shotcrete. Like FEBEX-DP and other international repository science activities, interactions with cementitious barrier materials (e.g., shotcrete) is important given its potential for alkaline reactions with other silicates (e.g., clay barriers, host rock) and the generation of high-pH pore solutions. These processes could lead to dissolution/precipitation processes at barrier interfaces that could affect solute (radionuclide) transport and clay barrier sorption properties.

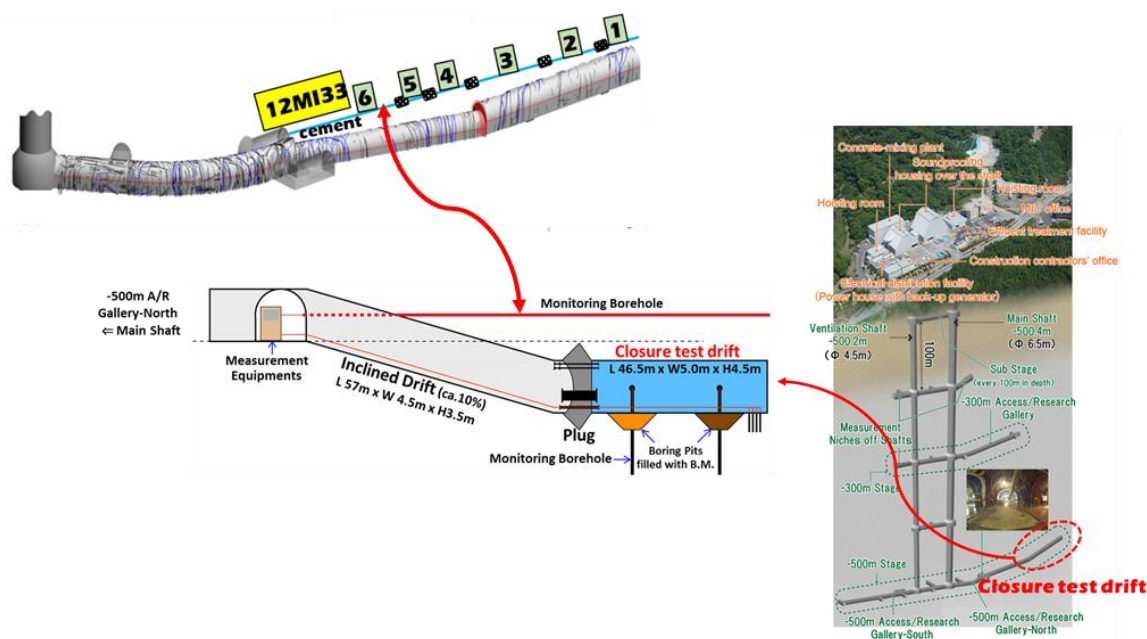


Figure 18. Diagrammatic picture of the closure test drift (CTD) at the Mizunami URL site, Japan. Upper schematic picture shows the inclined tunnel with CTD and the 12MI33 borehole with six monitoring zones. Figure content kindly provided by Dr. Teruki Iwatsuki (JAEA).

A 3D reactive transport representation has been implemented on a hydrological model of the site near the CTD. The goal is to extend the site hydrological model to capture the extent of high pH effects within the flooded tunnel and with distance from the cement-water interface. Such interactions in the water-filled zone may influence pore solution chemistry in the nearby monitoring boreholes where fractures in the excavated disturbed zone (EDZ) are present throughout the length of the CTD. Initial simulations involved the use of homogeneous permeability distributions to evaluate shotcrete liner interactions. The presented results make use of a hydrological model that includes heterogeneous permeability distributions to represent the effect of fractures along with the reactive transport model. The permeability distributions from the hydrological model only apply to the surrounding granite host-rock and not to the shotcrete liner in the tunnels. A homogeneous permeability of $1 \times 10^{-14} \text{ m}^2$ and porosity of 0.196 was assigned to the shotcrete liner.

The Visualization Area domain, which is a CTD-scale domain recommended by the project has been adopted. The domain size is 100 m x 150 m x 100 m. Mesh refinements were added around the CTD to capture the cement plug and the shotcrete on the walls of the CTD. The mesh size is now 70 x 302 x 75, resulting in 1,585,500 grid blocks. Figs. 19 and 20 show a slice along the axis of the tunnel and mesh refinements at the CTD, respectively, to allow modelling of the shotcrete and cement plug.

Fracture characterization was conducted using the method detailed in Wang et al. (2017). Measured fracture data from tunnel walls and from packer tests in monitoring wells were used to develop the

fracture model. A discrete fracture network (DFN) model was developed for the modelling domain for a selected number of realizations. For this study, the DFN “Realization 2” was used. The DFN permeability and porosity results for the selected realization were upscaled to the refined continuum mesh for use in flow and transport simulations. Figs. 21 and 22. show the upscaled permeability and porosity fields, respectively.

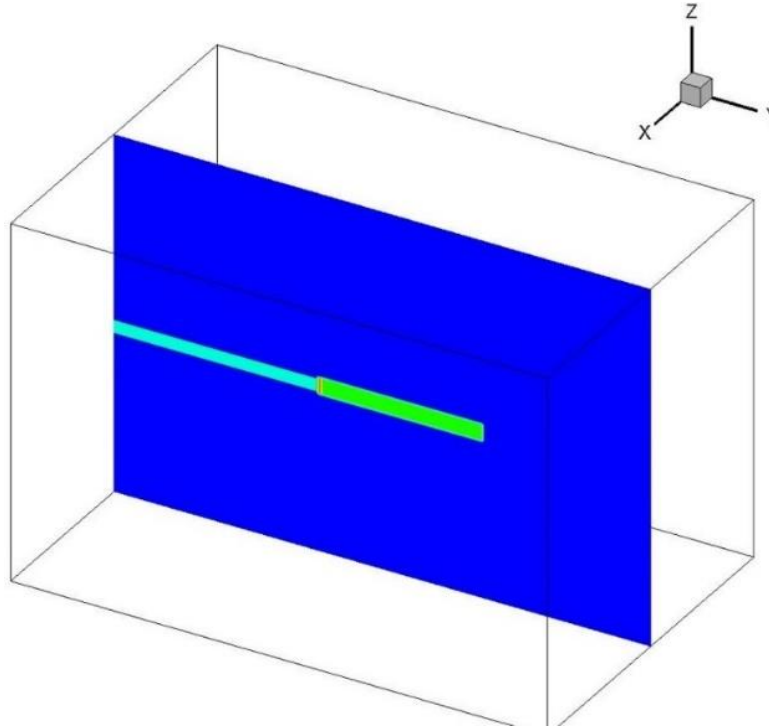


Figure 19. Vertical slice along the axis of the tunnel showing the CTD region (light green) and inclined drift (light blue).

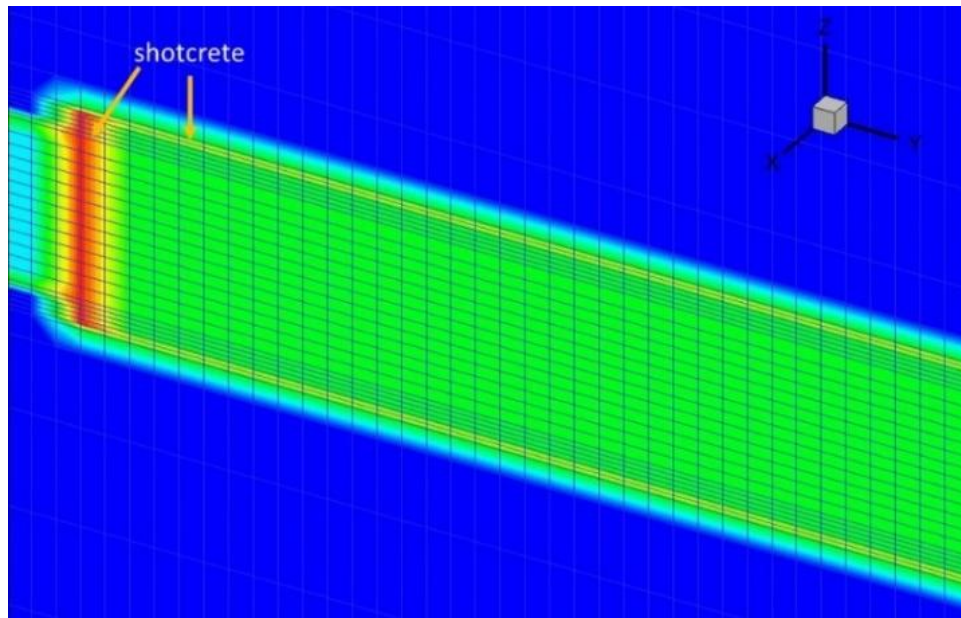


Figure 20. Mesh refinement showing shotcrete plug and lining around the CTD.

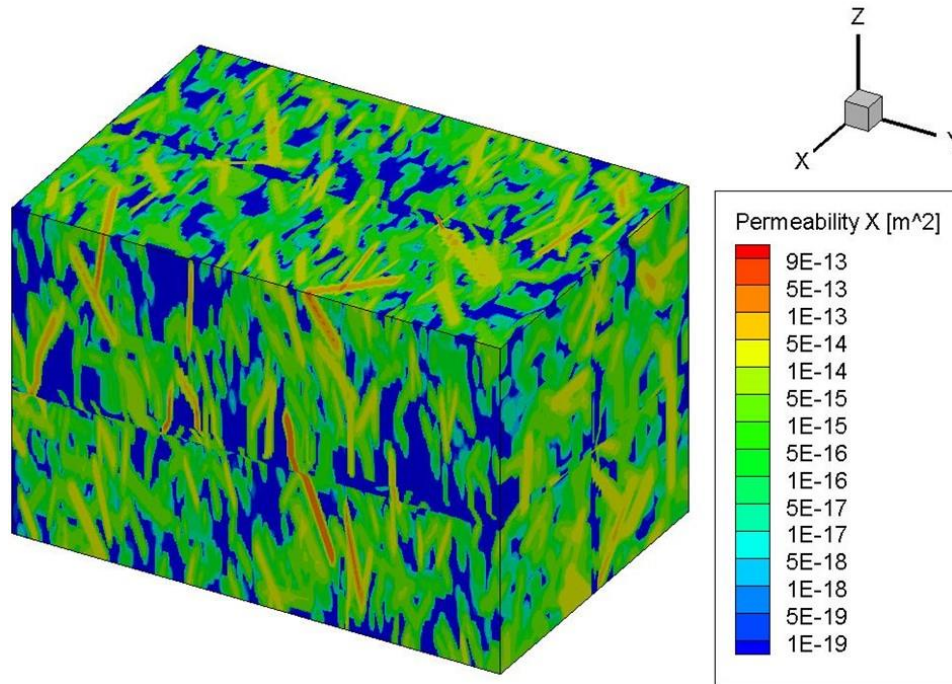


Figure 21. 3D domain representation of upscaled permeability field for DFN Realization 2.

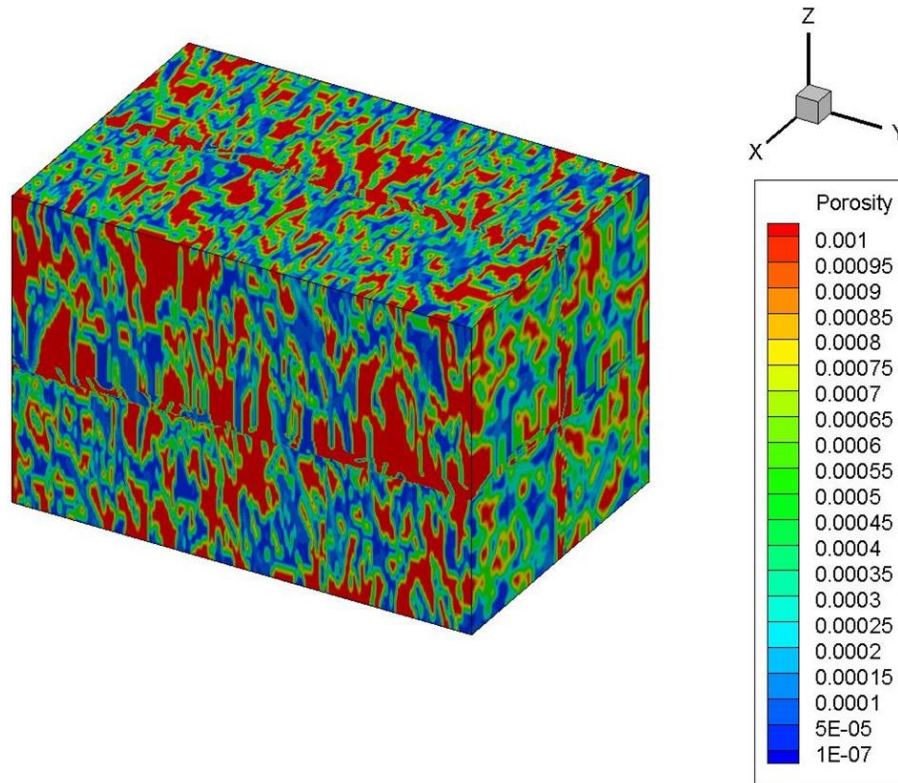


Figure 22. 3D domain representation of upscaled porosity field for DFN Realization 2.

The 3D reactive reactive-transport model implementation (Fig. 23) is done using the PFLOTRAN (Lichtner et al. 2019) simulator using similar parameters (e.g., material properties) to those adopted previously in the 1D evaluation of EBS material interactions (Jové Colón et al., 2016). The PFLOTRAN simulations were conducted in TH mode (coupled thermal-hydrological flow) assuming full saturation and transport by diffusion only. The diffusion constant adopted for these simulations is $2.2 \times 10^{-9} \text{ m}^2 / \text{s}$. Thermodynamic data for cementitious phases such as CSH(0.8, 1.6), portlandite, and ettringite were obtained from the THERMOPDEM database (Blanc et al., 2012; Blanc et al., 2006). The composition of the cementitious domain resembles that of ordinary Portland cement (OPC) assuming a calcite aggregate (Jové Colón et al., 2016). The current updated model considers a Cl-bearing phase (Friedel salt) and a Mg-bearing (brucite) in the cementitious phase assemblage. The reason for adding these phases is to account for their presence in the shotcrete and to evaluate their effect on solution chemistry, particularly on Cl concentration. The aggregate composition in the shotcrete was updated to include quartz and K-Na feldspars based on the analyses provided in the GREET website. Similar to the reactive transport simulations of the 12MI33 monitoring borehole, initial groundwater chemistry in the host rock above and below the CTD were constrained according to Iwatsuki et al. (2015).

Dissolution rate constants of cementitious solids were obtained from various sources as described in Jové Colón et al. (2016). As explained later in the text, rate law parameters for portlandite ($\text{Ca}(\text{OH})_2$) were adjusted to represent the observed pH and solute compositional trends at the CTD monitoring. The length of water-filled domain is about 47 m with a height of 5 m closely resembling the CTD dimensions. The thicknesses for the cement plug and shotcrete liner are 2 m and 0.1 m, respectively. The flooded CTD domain is represented by a porous medium having a porosity of almost unity and a very high permeability. The groundwater in the flooded domain is assumed to have the same chemistry as that of the host granitic rock. This groundwater chemistry also represents the starting solution chemistry of the filled CTD. The simulations were performed over a period of 300-600 days.

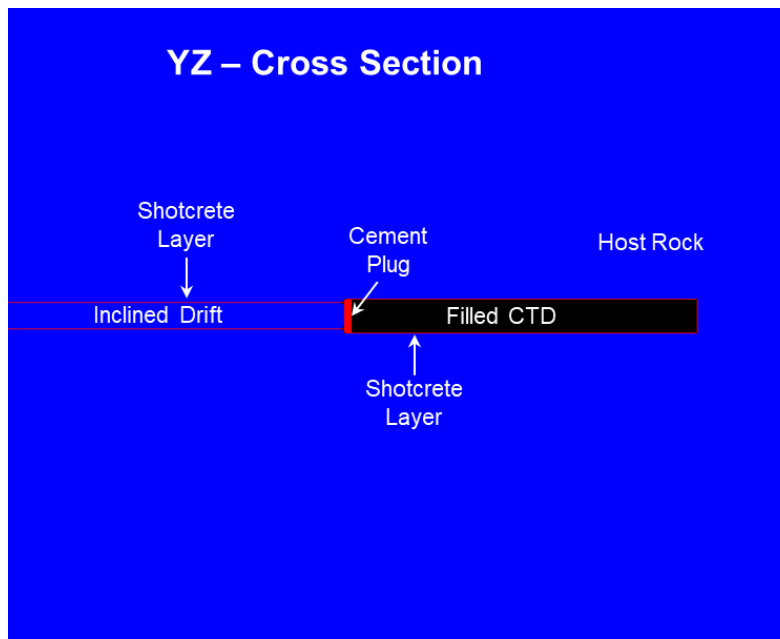


Figure 23. Schematic figure showing a YZ of the model domain in the PFLOTRAN reactive transport simulation of the CTD (black). Red areas delineate the shotcrete liner and cement plug. Observation points (not shown) are positioned at the tunnel length midpoint starting from the shotcrete-water interface up to a meter inside the water-filled tunnel.

Fig. 24 shows four time-snapshots (0, 60, 150, 300 days) of the pH mapping to represent the evolution of the reactive front from the shotcrete liner domain. As expected, pH increases with time from the interface into the water-filled CTD region and the host rock. After ~300 days of simulation time, the increase in pH because of the advancing front reaches ~0.5 m from the shotcrete interface into flooded CTD. About 1 m into the CTD, the pH remains close to the starting pH 8.9 for remainder of the simulation. The overall behavior of the reaction front described in these snapshots is very similar to that shown in Jové Colón et al. (2018, 2019).

The current stage of GREET effort involves the prediction of changes in groundwater chemistry to then be compared with data from monitoring boreholes from within the CTD and from the host rock within the excavated disturbed zone (EDZ). Fig. 25 (upper panel) shows the pH predictions from the PFLOTRAN reactive-transport model and the JAEA pH data. The measured pH data (purple dots connected by a line) show a rapid monotonic increase early in time then progressing towards a pH~10. Notice that measure pH data after 3/2016 show more variation with time (i.e., deviations from a monotonic increase) but still trending towards pH~10. The PFLOTRAN simulation results (solid curves) are shown for four observation points at approximate distances from the shotcrete interface (at the shotcrete interface, ~0.4 m, ~0.7 m, and ~1 m) into the flooded CTD. The model parameters utilized in Jové Colón et al. (2019) resulted in pH predictions at the observation point close to the shotcrete interface that underestimate the measured data at early times (<100 days). After 100 days, that same model resulted in good agreement with the measured pH trend progressing towards pH~10. The current PFLOTRAN update includes heterogeneous permeability and porosity fields in the host-rock (described earlier in the section) plus some variation in the reactive-transport model parameters to obtain an improved agreement with the measured pH at early times, but still predicting an increasing pH trend at later times. As in previous results, predictions at distances further from the shotcrete surface show a slower pH increase due to diffusive transport from the shotcrete interface into the filled CTD. This increase reaches pH~10.3 towards the end of the simulation which is close to the measured pH. Predictions of pH at ~1 m from the shotcrete interface show a relatively small increase with time indicating the limited effect of the reaction front on groundwater pH towards the tunnel center axis.

The JAEA pH data was used to conduct sensitivity analyses to constrain parameters in the transition state theory (TST) rate law in PFLOTRAN for portlandite dissolution kinetics (see Lichtner 2016). The observed trend in pH is assumed to be predominantly dependent on portlandite dissolution. This is expected considering that portlandite is the main leaching phase in the shotcrete interaction with groundwater. The adjusted parameters are related to the activities of primary chemical species (H^+ and Ca^{++}) in the prefactor term of the rate law pertaining the portlandite dissociation reaction. The overall agreement in the representation of the observed pH trend from the PFLOTRAN simulation suggests portlandite as the primary contributor to the pH change, even with the discrepancy at later times.

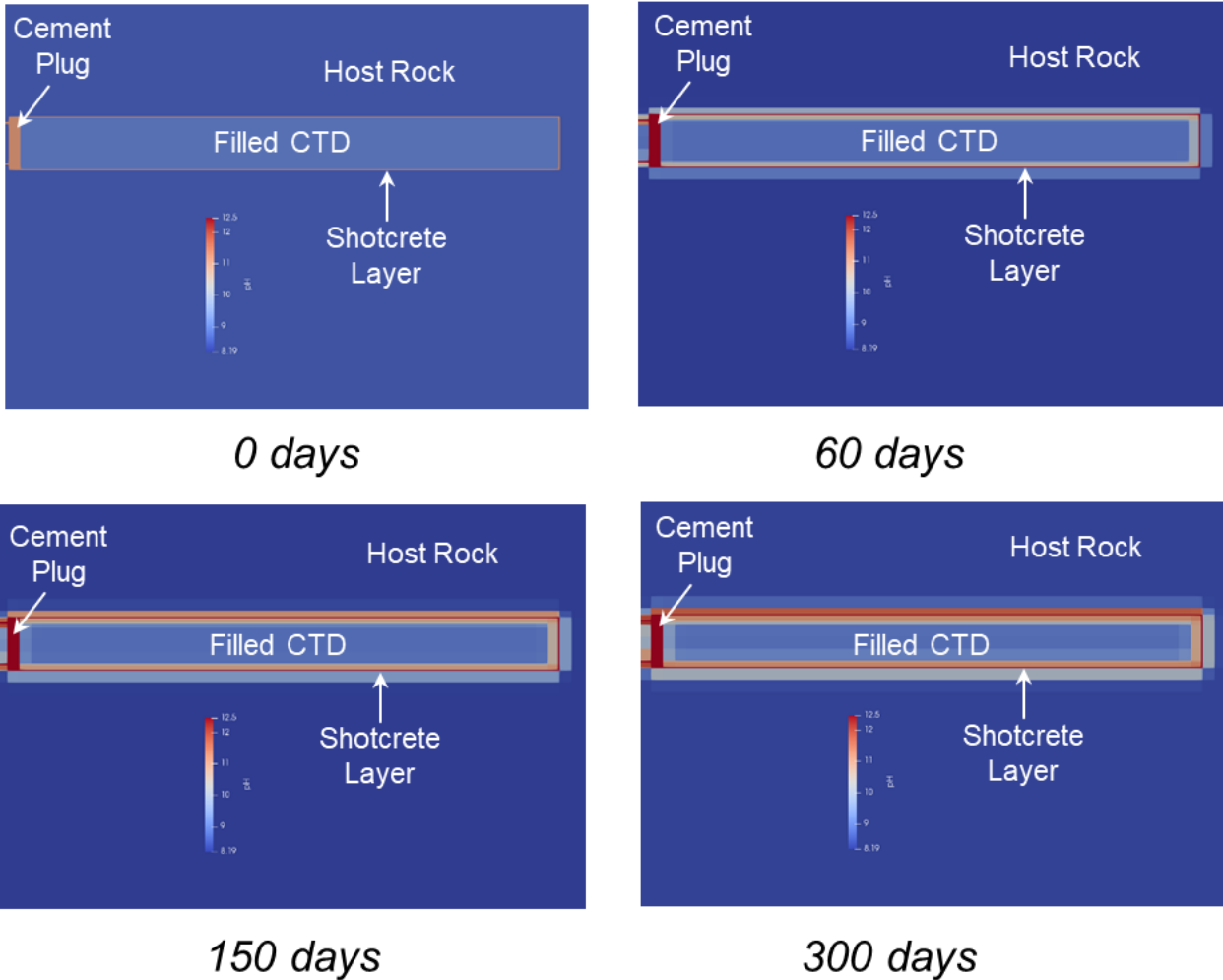


Figure 24. Predicted pH of the PFLOTRAN 3D reactive transport model of the CTD and surrounding host rock. The reaction front diffuses into the CTD and into host rock. pH color map scale ranges from 8.19 to 12.5.

Sensitivity analysis were conducted to evaluate the effects of dissolution kinetics, potential for other phases contributing to the overall pH change, volume fractions of reactants, and transport parameters. It appears that portlandite dissolution rate law parameters, diffusion rate, and thickness of the shotcrete liners are the most important to produce the pH trend. The effects of some of these parameters are discussed later in the section.

Fig. 25 shows the JAEA measured concentration of Na^+ (lower panel) decreasing with time with some level of scatter. The PFLOTRAN parameters used in Jové Colón et al. (2019) resulted in a decrease in temporal Na^+ concentration predictions near the shotcrete interface in good agreement with the overall measured trend. However, simulation results with updated parameters shows the measured Na^+ concentration (lower panel) decreasing with time with some level of scatter. The PFLOTRAN predictions at the shotcrete interface indicate a sudden decrease of Na^+ concentration with time with a subsequent increase at $t > 100$ days. This initial dip in the simulation prediction is off trend with the measured data even when it recovers at subsequent times. The subsequent increase in Na^+ concentration with time is consistent with initial porewater Na^+ concentrations in the rock below the CTD region. This is indicative of the effects of groundwater mixing between the CTD and the

host-rock through the shotcrete liner. Other simulations with different constrains have shown better agreement with the overall measured Na concentrations but at the compromise of not having a good representation of the measured pH trend at early times. The predictions of temporal changes in Na⁺ concentration with distance from the shotcrete interface show similar decreasing profiles but with the expected effect of a slow moving front away from the shotcrete surface in the flooded CTD. It is inferred that simulation predictions obtained at a distance between the shotcrete interface and ~0.4m would produce a trend that should be in better agreement with at least part of the data. However, the mesh cell discretization in these domains is not sufficiently fine to sample observation points at such intervals. Finer mesh discretizations of the shotcrete domain were attempted but the large computational burden and memory size limitations prevented from either having successful simulations or code runs within a reasonable period of time – even when using high performance computing (HPC) platforms.

Fig. 26 shows the temporal evolution of Ca⁺⁺ and Cl⁻ concentrations in the CTD. Notice that both aqueous component concentrations show an initial ($t \leq \sim 150$ days) sharp decrease to subsequently attain a nearly steady-state concentration. The PFLOTRAN simulation does produce an initial decrease in both Ca⁺⁺ and Cl⁻ close to the shotcrete interface observation point. However, similar to the Na⁺ concentration profile, the Ca⁺⁺ and Cl⁻ concentrations initially drop reaching a minimum with a subsequent increase towards the end of the simulation. Such an initial large decrease is caused by mixing of groundwater, shotcrete porewater, and CTD water and/or Cl⁻ uptake by precipitation of a Cl-bearing cementitious phase. The subsequent increase in Cl⁻ concentration by the mixing influence of the porewaters in the host-rock below the CTD through the shotcrete liner. It should be noted that calcite is predicted to form in the shotcrete liner but in relatively small amounts and could also contribute in controlling Ca⁺⁺ concentration in the porewater. The formation of calcite in shotcrete has been reported by the GREET project. These observations need further evaluation through monitoring and phase characterization activities, along with reactive transport simulations, for example, focusing on evaluating the effects of hydrological characteristics (porosity and permeability) in shotcrete and host rock.

The predicted pH and solute concentration profiles are indicative of strong mixing effects due to fluid transport between host-rock groundwater, shotcrete liner pore solution, and CTD water chemistry. To test this idea, the thickness of the shotcrete was increased from 10 cm to 20 cm. This is double the shotcrete thickness relative to what was considered nominal for the CTD but it would then cover the desired length scales for thickness in this test. Also, the reactive surface area of portlandite was decreased from 1 m²/m³ to 0.1 m²/m³. The diffusion constant was decreased from 2.2×10^{-9} m²/s to 8.5×10^{-10} m²/s. All other parameter values including mineral volume fractions were kept unchanged.

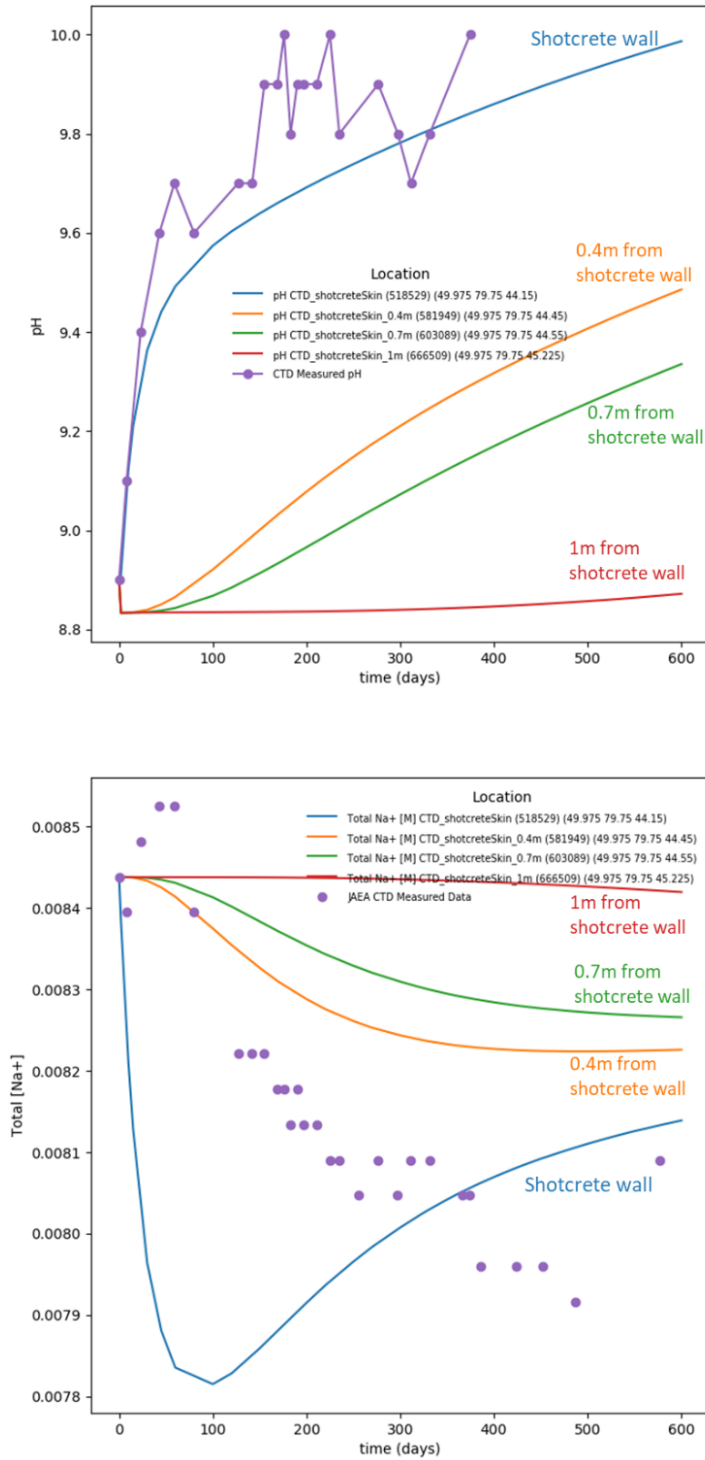


Figure 25. Measured and predicted pH (upper panel) and Na⁺ concentration (lower panel) in moles/L profiles at the midpoint region of the CTD and shotcrete thickness of 10 cm. Actual distances from the shotcrete surface labeled in the plot as “Shotcrete wall”, 0.4 m, 0.7 m, and 1 m correspond to 5 cm, 35 cm, 45 cm, and 1.1 cm, respectively.

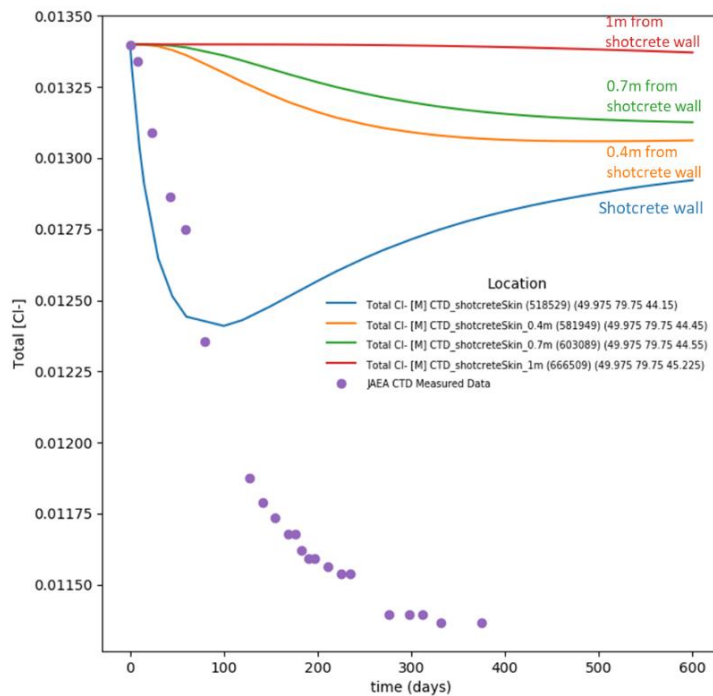
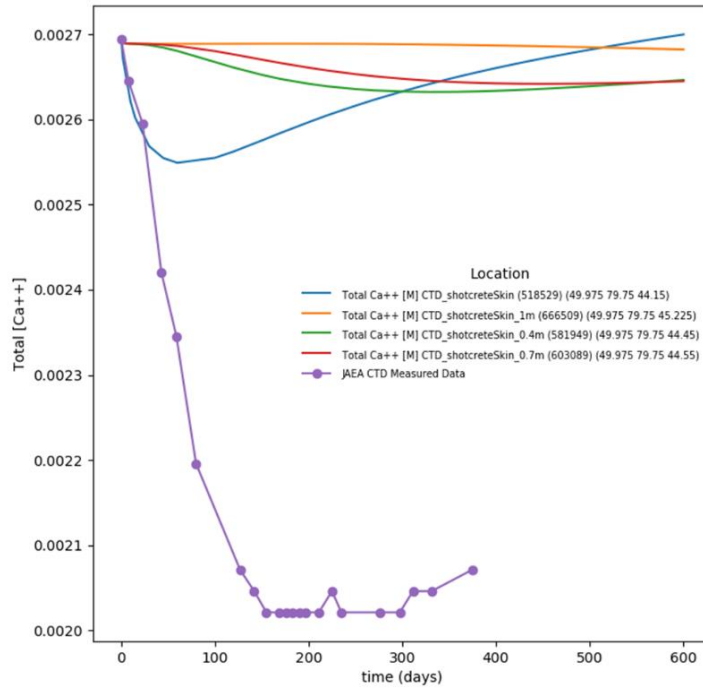


Figure 26. Measured and predicted Ca^{++} (upper panel) and Cl^- concentration (lower panel) profiles in moles/L at the midpoint region of the CTD and shotcrete thickness of 10 cm. Actual distances from the shotcrete surface labeled in the plot as “Shotcrete wall”, 0.4 m, 0.7 m, and 1 m correspond to 5 cm, 35 cm, 45 cm, and 1.1 cm, respectively.

Fig. 27 shows the temporal evolution of pH and Na^+ concentration in the CTD for a shotcrete thickness of 20 cm. The agreement between simulated and measured data for the pH vs. time profile is significantly improved with the latest changes in parameters. On the other hand, the predicted Na^+ concentration trend for the observation point near the shotcrete surface underestimate the measured data. However, the simulation generates a trend similar to the measured data. Even with this discrepancy, the differences are not large considering the scale of concentration values. Interestingly, the predicted Na^+ concentration at ~ 0.2 m produces a trend that is in very good agreement with the measured values. The reason for this agreement cannot be resolved at this moment. Fig. 28 shows the predicted Ca^{++} and Cl^- concentrations as a function of time showing very good agreement with measured values at early times. However, the simulations slightly overestimate the measured values at later times but maintaining the same trend. Similar to Na^+ , these differences are not large considering the scale of concentration values.

It should be emphasized that the change in shotcrete thickness and some changes in simulation parameters relative to those for a 10 cm thickness generate results that not only are in better agreement with the measured data for the considered solutes but more importantly, it generates concentration trends that conforms to the observe values. This indicates the sensitivity of the modeled system to transport length scales, mixing, and its coupled effect on the aqueous chemistry of major solutes. It also indicates the importance of leaching of key cementitious phases like portlandite in controlling primarily pH and Ca concentrations. The latter form complexes with Cl in solution and through the mixing with the CTD water it could produce Cl-bearing secondary phases like Friedel salt which was observed in the shotcrete.

All these results have provided key information in the buildup of a 3D H-C model for the GREET project. For example, the use of heterogeneous porosity and permeability distributions to account for fracture flow effects in the host rock and potential effects on reactive transport between the CTD and its surroundings. It also allows for the evaluation of groundwater mixing close to the shotcrete-rock domain and its effect on CTD water chemistry. Further, sensitivity analyses on rate law and transport parameters are used to analyze their impact on pH and predicted solute concentrations as a function of time gauged by water chemistry measurements. These analyses are based on rather unique URL borehole monitoring and water sampling activities that provide key information to test these models.

These modeling results are very encouraging in providing a coupled HC process model addressing a challenging field experiment and generating predictions that are in good agreement with measurements. It also serves as a test bed for the application of HPC to assess large scale problems in 3D where EBS material interaction with fluids plays a key role in describing near-field chemistry and hence the safety performance of the disposal design concept.

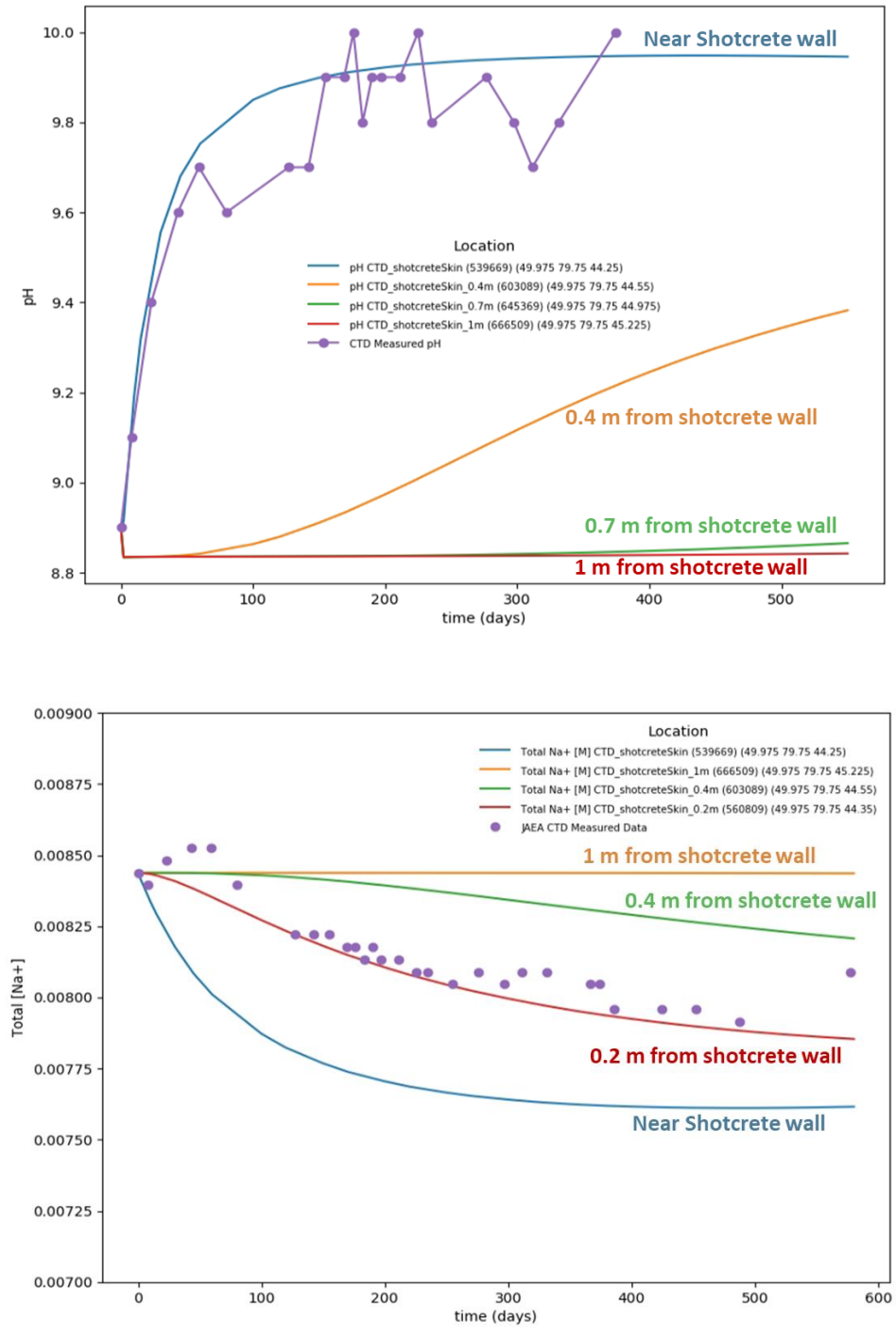


Figure 27. Measured and predicted pH (upper panel) and Na⁺ concentration (lower panel) in moles/L profiles at the midpoint region of the CTD and shotcrete thickness of 20 cm. Actual distances from the shotcrete surface labeled in the plot as “Near shotcrete wall”, 0.2 m, 0.4 m, and 1 m correspond to 5 cm, 15 cm, 35 cm, and 1.02 m, respectively.

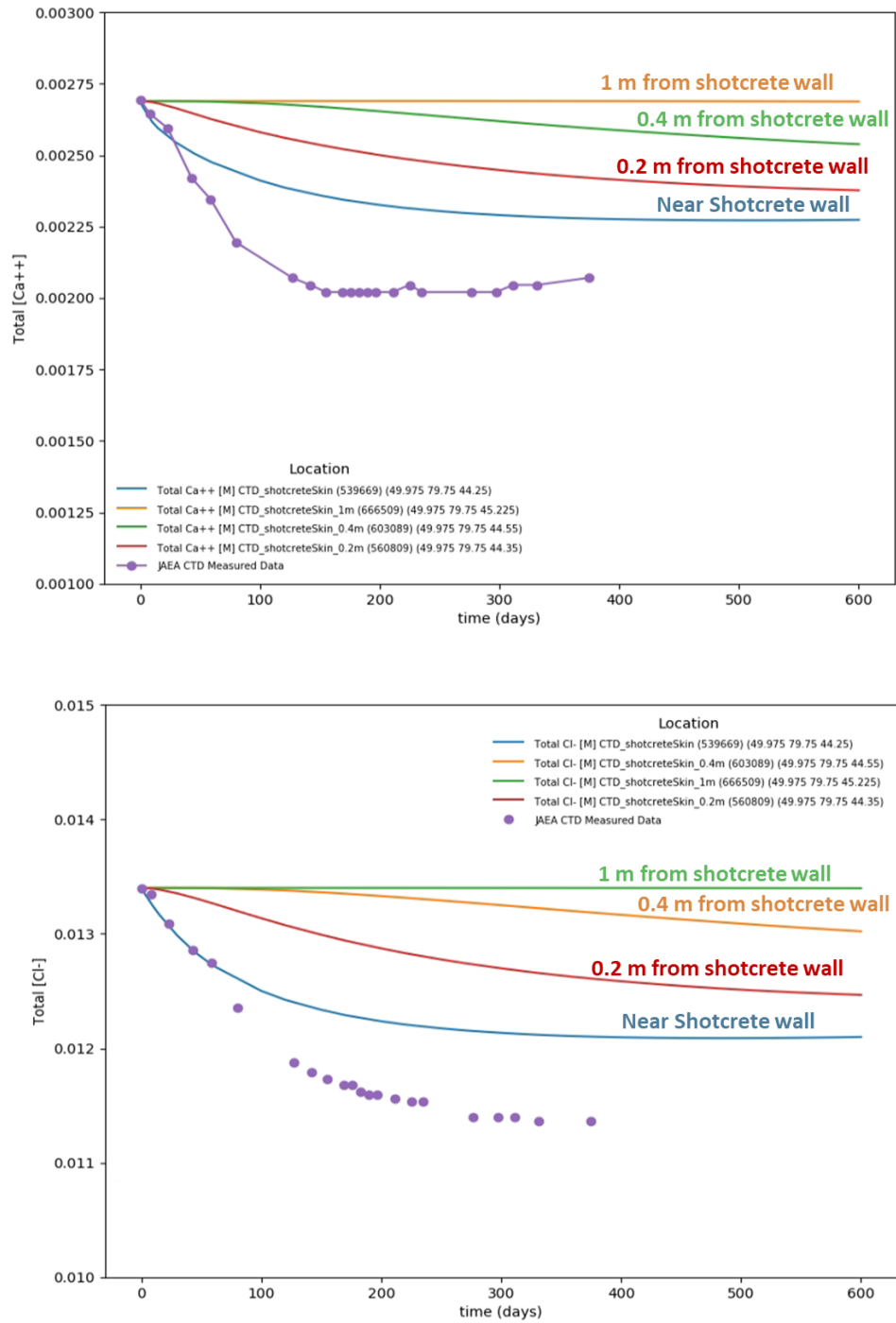


Figure 28. Measured and predicted Ca^{++} (upper panel) and Cl^- concentration (lower panel) profiles in moles/L at the midpoint region of the CTD and shotcrete thickness of 20 cm. Actual distances from the shotcrete surface labeled in the plot as “Near shotcrete wall”, 0.2 m, 0.4 m, and 1 m correspond to 5 cm, 15 cm, 35 cm, and 1.02 m, respectively.

All these ongoing results have provided key information in the buildup of a 3D H-C model. The use of heterogeneous porosity and permeability distributions to account for fracture flow effects in the host rock and potential effects on reactive transport between the CTD and its surroundings. For example, evaluation of groundwater mixing close to the shotcrete-rock domain and its effect on CTD water chemistry. Sensitivity analyses on rate law and transport parameters to analyze their impact on pH and predicted solute concentrations as a function of time. These analyses are based on URL borehole monitoring and water sampling activities that provide key information to rest these models.

VII. Conclusions

- **FEBEX-DP:**
 - Results of cyclical TGA/DSC thermal analyses under controlled RH (hydration/dehydration) and constant temperature for Section 49 samples with different grain sizes are similar to those obtained previously for bulk bentonite. The cyclical data indicates that the dehydration behavior is a function of the duration of hydration that precedes it. The appearance of a “shoulder peak” during dehydration suggests different energetics for swelling clay hydration and dehydration processes. The latter results in the slower removal of water and potentially giving rise to the observed hysteretic behavior in water sorption experiments. Preliminary results of MD simulations indicate a slower water removal when there is less than one water (1W) of hydration at the montmorillonite interlayer. Therefore, differences in water transport and confinement mechanisms in expansive clay can influence chemo-mechanical behavior in response to changes in thermal and hydration/dehydration conditions.
 - Experiments of FEBEX-DP bentonite interactions FeCl_2 shows destabilization of the clay phase as expected. Experiments at 200°C show evidence of clay dissolution and potential exchange with Fe. However, there is no clear evidence for illitization, significant clay phase transformation, or secondary mineralization based on preliminary XRD analyses of run products.
- **DECOVALEX-2019 Task C of GREET Experiment** – 3D reactive transport modeling of the CTD and effects of shotcrete liner:
 - 3D PFLOTRAN reactive transport modeling of shotcrete liner interaction was conducted using a hydrological model of the site domain focusing on the CTD field experiment.
 - A TST kinetic rate law for dissolution of the portlandite phase in shotcrete was used with parameters adjusted to represent measured pH and solute concentrations. PFLOTRAN predictions of pH and selected solutes (Ca, Na, Cl) concentrations with time at midpoint length of the CTD, close to the shotcrete interface, are in general agreement with the measurements. However, the predicted concentrations of major solutes such as Ca^{++} and Cl^- concentrations tend to slightly overestimates the measured data.
 - Better agreement with the measured pH and solute data trends is obtained with a shotcrete thickness of 20 cm – twice the thickness of that considered in the initial case. This suggest how sensitivity the modeled system is to transport length scales, mixing, and the coupling of these effects on the aqueous chemistry of major solutes for reaction with shotcrete material.

- Groundwater mixing/dilution combined with Cl^- complexation uptake by precipitation of a Cl^- -bearing phase (e.g., Friedel's salt) was investigated to evaluate the observed decrease in Cl^- concentration with time. The presence of this Cl^- -bearing phase was not sufficient to represent the observed initial drop in Cl^- concentration.

VIII. FY21 Work

Planned work on **FEBEX-DP** samples for FY21 (and the remainder of FY20):

- Continue cyclical thermal analyses conducted at a higher constant temperature and RH to evaluate the effect on hydration/dehydration profiles. Conduct XRD analyses under controlled RH and temperature conditions to complement cyclical TGA/DSC analyses.
- Expand MD simulations on dehydration phenomena at the clay interlayer. Potential work includes conducting Monte Carlo (MC) and MD to evaluate the energetics of the system at different water contents.
- Continue investigations on FEBEX bentonite interactions with FeCl_2 solutions to evaluate effects on clay stability and data interpretation.

Planned work on **DECOVALEX** work for FY21 (and the remainder of FY20):

- Prepare manuscript describing the 3D reactive-transport modeling work on DECOVALEX-2019 Task C (GREET) emphasizing on modeling the CTD chemical data highlighting the effects of shotcrete leaching and transport parameters on the resulting temporal evolution of solute concentration profiles.
- DECOVALEX-2019 phase has ended and is moving towards the next phase DECOVALEX-2023. Work on the new DECOVALEX phase will be focused on the new tasks of interest for disposal in argillite work package which are still under review.

IX. References

Birkholzer, J., Faybishenko, B., Ajo-Franklin, J., Borglin, S., Dobson, P., Gilbert, B., Guglielmi, Y., Fox, P.M., Kim, K., Nico, P., Rutqvist, J., Sonnenthal, E., Xu, H., Wu, Y., Zheng, L., Caporuscio, F.A., Reimus, P., Viswanathan, H., Jove-Colon, C.F., Wang, Y., Kuhlman, K., Matteo, E., McMahan, K. and Zavarin, M. (2019) International Collaboration Activities in Different Geologic Environments, Spent Fuel Waste Science and Technology (SFWST) Deliverable M2SF-19LB010307012 (LBNL-2001239). Lawrence Berkeley National Laboratories (LBNL), Berkeley, CA USA, 356 pp..

Birkholzer, J., B. Faybishenko, P.F. Dobson, P. M., J. Rutqvist, L. Zheng, F.A. Caporuscio, P. Reimus, H. Viswanathan, C.F. Jove-Colon, Y. Wang, K. Kuhlman, E. Matteo, K. McMahan, and M. Zavarin, 2018. International Collaboration Activities in Different Geologic Environments, in Spent Fuel Waste Science and Technology (SFWST) Deliverable M2SF-18LB010307012 (LBNL-2001178), Lawrence Berkeley National Laboratories (LBNL): Berkeley, CA USA. 298 pp.

Birkholzer, J., Faybishenko, B., Zheng, L., Rutqvist, J., Dobson, P., Fox, P.M., Reimus, P., Viswanathan, H., Jove-Colon, C.F., Wang, Y., Kuhlman, K., McMahan, K. and Zavarin, M., 2017. International Collaboration Activities in Different Geologic Disposal Environments (SFWD-SFWST-2017-000013), Prepared for US Department of Energy, Spent Fuel and Waste Disposition Campaign (SFWD-SFWST-2017-000013). (National Laboratory Report No. LBNL-2001063), Berkeley, California, pp. 236 pp.

- Blanc, P., Lassin, A., Piantone, P., Azaroual, M., Jacquemet, N., Fabbri, A. and Gaucher, A., 2012. Thermoddem: A geochemical database focused on low temperature water/rock interactions and waste materials. *Applied Geochemistry*, 27: 2107-2116.
- Blanc, P., Piantone, P., Lassin, A. and Burnol, A., 2006. Thermochimie: Sélection de constantes thermodynamiques pour les éléments majeurs, le plomb et le cadmium, Rapport final BRGM/RP-54902-FR BRGM, France, pp. 1-157.
- Cheshire, M.C., Caporuscio, F.A., Jové Colón, C.F., and Norskog, K.E. (2018). "Fe-saponite growth on low-carbon and stainless steel in hydrothermal-bentonite experiments." *Journal of Nuclear Materials* 511: 353-366.
- Friedrich, F., Schild, D., Weidler, P.G. and Schäfer, T., 2016. Hydration of FEBEX Bentonite as Observed by Environmental Scanning Electron Microscopy (ESEM), Filling the Gaps - From Microscopic Pore Structures to Transport Properties in Shales. The Clay Minerals Society Workshop Lectures Series. The Clay Minerals Society, Virginia, USA, pp. 199-210.
- García-Siñeriz, J.L., Abós, H., Martínez, V., De la Rosa, C., Mäder, U. and Kober, F., 2016. FEBEX DP: Dismantling of heater 2 at the FEBEX "in situ" test: Description of operations - Arbeitsbericht NAB 16-11, National Cooperative for the Disposal of Radioactive Waste (NAGRA), Wettingen, Switzerland.
- Grim, R.E., 1968. Clay mineralogy. International series in the earth and planetary sciences. McGraw-Hill, New York.
- Huertas, F., Fuentes-Cantillana, J.L., Jullien, F., Rivas, P., Linares, J., Fariña, P., Ghoreychi, M., Jockwer, N., Kickmaier, W., Martínez, M.A., Samper, J., Alonso, E. and Elorza, F.J., 2000. Full-scale engineered barriers experiment for a deep geological repository for high-level radioactive waste in crystalline host rock (FEBEX project): Final report. EUR 19147, European Commission, Brussels.
- Iwatsuki, T., Furue, R., Mie, H., Ioka, S. and Mizuno, T., 2005. Hydrochemical baseline condition of groundwater at the Mizunami underground research laboratory (MIU). *Applied geochemistry*, 20(12): 2283-2302.
- Iwatsuki, T., Hagiwara, H., Ohmori, K., Munemoto, T. and Onoe, H., 2015. Hydrochemical disturbances measured in groundwater during the construction and operation of a large-scale underground facility in deep crystalline rock in Japan. *Environmental Earth Sciences*, 74(4): 3041-3057.
- Iwatsuki, T., Munemoto, T., Kubota, M., Hayashida, K. and Kato, T., 2017. Characterization of rare earth elements (REEs) associated with suspended particles in deep granitic groundwater and their post-closure behavior from a simulated underground facility. *Applied Geochemistry*, 82: 134-145.
- Jové Colón, C.F., Payne, C., Coker, E., Boisvert, L., Sanchez, A., Knight, A. and Hadgu, T. (2019) Argillite Disposal R&D International Collaborations interim report - 2019 (SAND2019-6731 R), Prepared for U.S. Department of Energy (DOE) Spent Fuel Waste Science and Technology (SFWST). Sandia National Laboratories, Albuquerque, New Mexico, 51 pp.
- Jové Colón, C.F., C. Payne, and A. Knight, 2018. International Collaboration Activities on Disposal in Argillite R&D: Progress Report, in Spent Fuel Waste Science and Technology Deliverable M4SF18SN010301092 (SAND2018-9718 R), Sandia National Laboratories: Albuquerque, New Mexico USA. p. 51.

Jové Colón, C.F., Hammond, G.E., Kuhlman, K., Zheng, L., Kim, K., Xu, H., Rutqvist, J., Caporuscio, F.A., Norskog, K.E., Maner, J., Palaich, S., Cheshire, M., Zavarin, M., Wolery, T.J., Atkins-Duffin, C., Jerden, J.L., Copple, J.M., Cruse, T. and Ebert, W.L., 2016. Evaluation of Used Fuel Disposition in Clay-Bearing Rock (FCRD-UFD-2016-000074), Sandia National Laboratories, Albuquerque, NM. SAND2016-10311 R.

Lichtner, P.C., 2016, Kinetic rate laws invariant to scaling the mineral formula unit. *American Journal of Science*, 316(5): p. 437-469.

Lichtner, P. C., et al. (2019). PFLOTRAN user manual: A massively parallel reactive flow and transport model for describing surface and subsurface processes. <http://documentation.pflotran.org>

Martinez, V., Abós, H. and García-Siñeriz, J.L., 2016. FEBEXe: Final Sensor Data Report (FEBEX "in situ" Experiment) - Arbeitsbericht NAB 16-19, National Cooperative for the Disposal of Radioactive Waste (NAGRA), Wettingen, Switzerland.

Marty, N.C.M., Bildstein, O., Blanc, P., Claret, F., Cochapin, B., Gaucher, E.C., Jacques, D., Lartigue, J.E., Liu, S.H., Mayer, K.U., Meeussen, J.C.L., Munier, I., Pointeau, I., Su, D.Y. and Steefel, C.I., 2015. Benchmarks for multicomponent reactive transport across a cement/clay interface. *Computational Geosciences*, 19(3): 635-653.

McKay, J., 1992. Clay Separation. LSIS Technical Memorandum #92-1. University of Western Ohio.

Missana, T. and García-Gutiérrez, M., 2007. Sorption of bivalent ions (Ca (II), Sr (II) and Co (II)) onto FEBEX bentonite. *Physics and Chemistry of the Earth, Parts A/B/C*, 32(8): 559-567.

Montes-H, G., J. Duplay, L. Martinez, Y. Geraud, and B. Rousset-Tournier, Influence of interlayer cations on the water sorption and swelling–shrinkage of MX80 bentonite. *Applied Clay Science*, 2003a. 23(5-6): p. 309-321.

Montes-H, G., J. Duplay, L. Martinez, and C. Mendoza, Swelling–shrinkage kinetics of MX80 bentonite. *Applied Clay Science*, 2003b. 22(6): p. 279-293.

Muurinen, A., 2011. Measurements on Cation Exchange Capacity of Bentonite in the Long-Term Test of Buffer Material (LOT), Working Report 2011-10. POSIVA, Eurajoki, Finland, pp. 30.

Plimpton, S. (1995). "Fast Parallel Algorithms for Short-Range Molecular Dynamics." *J Comp Phys* 117: 1-19.

Tajeddine, L., Gailhanou, H., Blanc, P., Lassin, A., Gaboreau, S. and Vieillard, P., 2015. Hydration–dehydration behavior and thermodynamics of MX-80 montmorillonite studied using thermal analysis. *Thermochimica Acta*, 604: 83-93.

Teich-McGoldrick, S.L., Greathouse, J.A., Jové-Colón, C.F. and Cygan, R.T., 2015. Swelling Properties of Montmorillonite and Beidellite Clay Minerals from Molecular Simulation: Comparison of Temperature, Interlayer Cation, and Charge Location Effects. *The Journal of Physical Chemistry C*, 119(36): 20880-20891.

Vieillard, P., Tajeddine, L., Gailhanou, H., Blanc, P. and Lassin, A., 2016. Thermo-Analytical Techniques on MX-80 Montmorillonite: A Way to Know the Behavior of Water and its Thermodynamic Properties during Hydration–Dehydration Processes. *Pharm Anal Acta*, 7: 462.

Villar, M.V., Fernandez, A.M., Romero, E., Dueck, A., Cuevas, J., Plotze, M., Kaufhold, S., Dohrmann, R., Iglesias, R.J., Sakaki, T., Voltolini, M., Zheng, L., Kawamoto, K. and Kober, F., 2017. FEBEX-DP Post-mortem THM/THG Analysis Report, NAGRA Arbeitsbericht NAB 16-17. NAGRA, Wettingen, Switzerland, pp. 187 pp.

Wang, Y., T. Hadgu, E. A. Kalinina, J. Jerden, V. K. Gattu, W. Ebert, H. Viswanathan, J. Hyman, S. Karra, N., Knapp, N. Makedonska, P. Reimus, K. Telfeyan, P. M. Fox, P. S. Nico, M. Zavarin, E. Balboni, and C. Atkins-Duffin: Evaluation of Spent Fuel Disposition in Crystalline Rocks: FY17 Progress Report, Spent Fuel and waste Disposition, SFWD-SFWST-2017-000007, September, 2017.

Wilson, J.C., Benbow, S., Sasamoto, H., Savage, D. and Watson, C., 2015. Thermodynamic and fully-coupled reactive transport models of a steel-bentonite interface. *Applied Geochemistry*.

Xie, M.L., Mayer, K.U., Claret, F., Alt-Epping, P., Jacques, D., Steefel, C., Chiaberge, C. and Simunek, J., 2015. Implementation and evaluation of permeability-porosity and tortuosity-porosity relationships linked to mineral dissolution-precipitation. *Computational Geosciences*, 19(3): 655-671.

X. APPENDIX A

TGA/DSC Data

Selected FEBEX-DP Bentonite Samples – Section 49

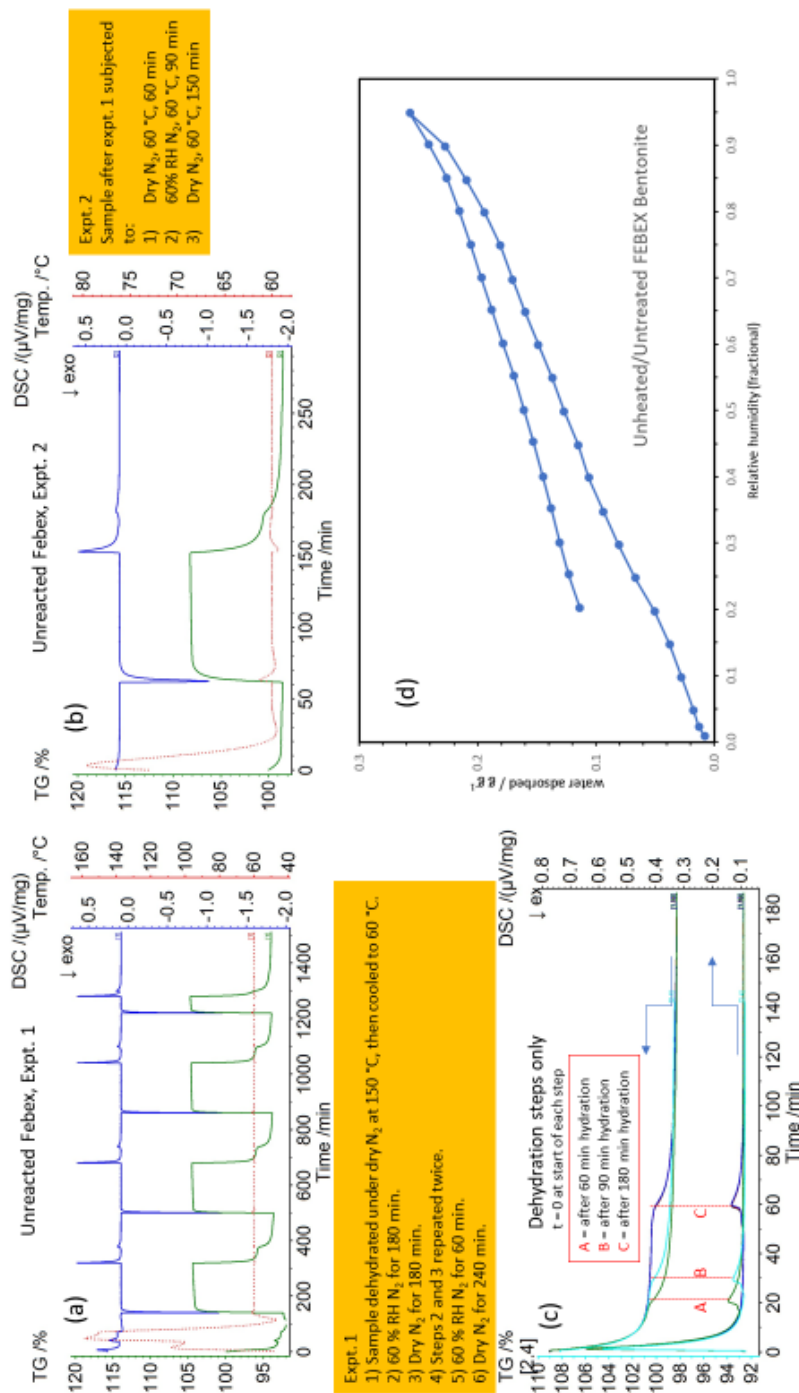


Figure A-1. TGA/DSC curves as a function of time (minutes) for water adsorption/desorption cycles at 60°C for unheated (baseline) FEBEX bentonite (two thermal experiments). (a) and (b) Experiments 1 and 2, respectively: the green curve represents the thermogravimetric analysis (left y-axis). The blue curve stands for the DSC analysis (right y-axis). The red dotted line signifies the temperature (2nd right y-axis). See Fig. 7 in the text for explanation of hydration/dehydration cycles. (c) DSC measurements as a function of elapsed time for the dehydration interval showing the shifts in the second peak or “dehydration shoulder” for hydration time durations of 60 and 180 minutes. (d) Water adsorption/desorption isotherms at 20°C for unheated/untreated FEBEX bentonite.

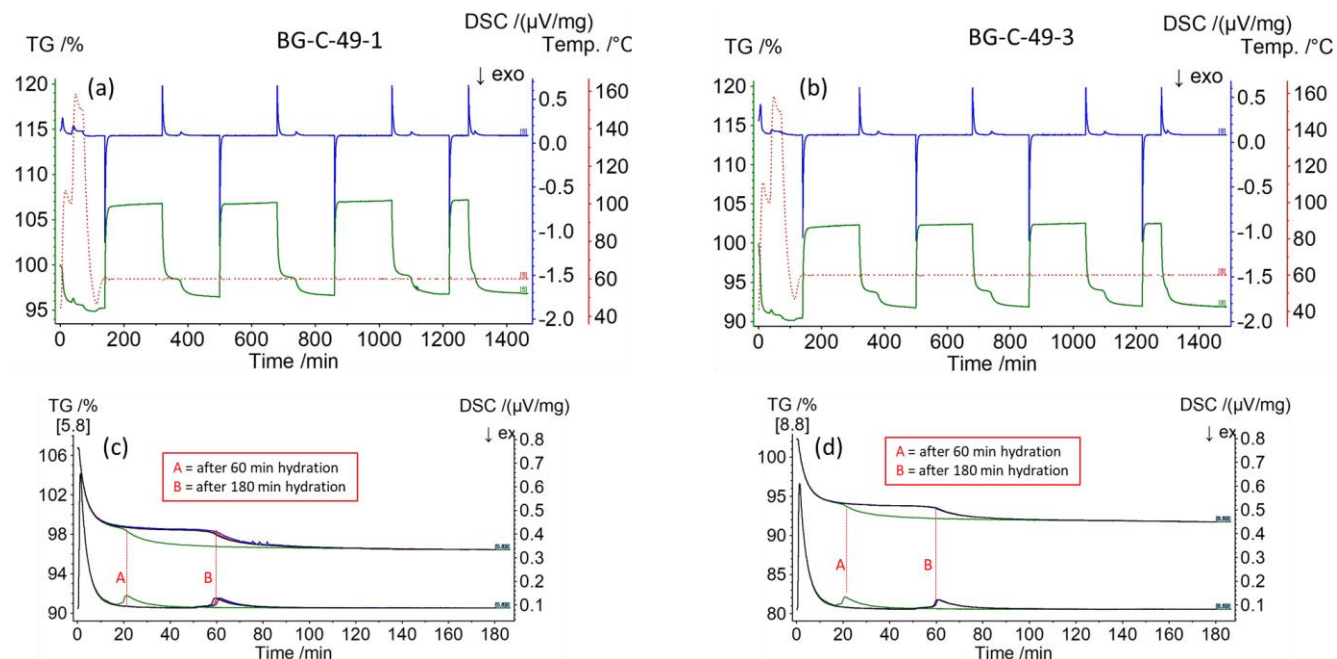


Figure A-2. TGA/DSC curves as a function of time (minutes) for water adsorption/desorption cycles at 60°C for FEBEX-DP bentonite samples BG-C-49-1 (a) and BG-C-49-3 (b). The green curve represents the thermogravimetric analysis (left y-axis). The blue curve stands for the DSC analysis (right y-axis). The red dotted line signifies the temperature (2nd right y-axis). (c) and (d); corresponding TGA/DSC curves as a function of time (minutes) for dehydration cycles only at the time interval of the appearance of the second peak or “dehydration shoulder”. See Fig. 7 in the text for explanation of hydration/dehydration cycles. DSC measurements show the peak shifts (A and B) for the dehydration time interval in response to hydration duration.

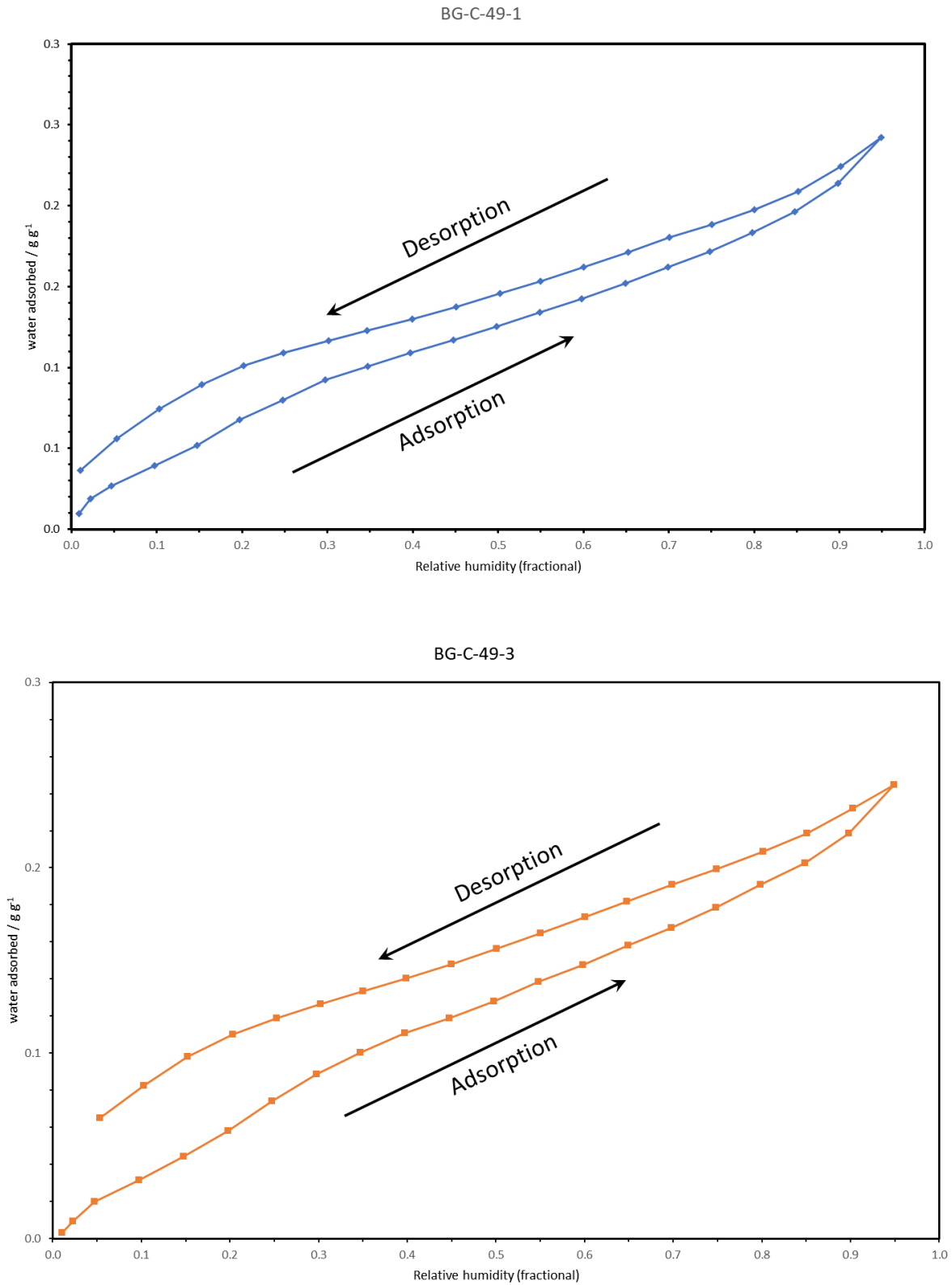


Figure A-3. Volumetric water sorption/desorption isotherms obtained at 20°C for samples BG-C-49-1 and BG-C-49-3.

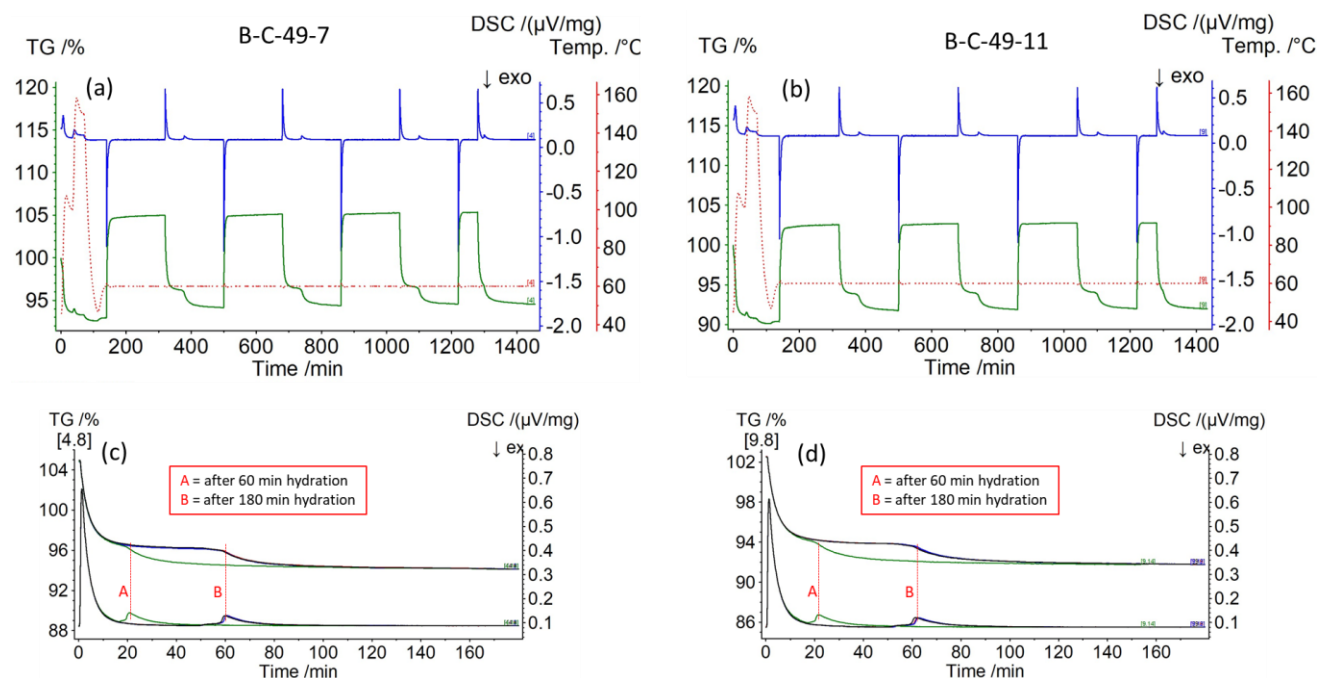


Figure A-4. TGA/DSC curves as a function of time (minutes) for water adsorption/desorption cycles at 60°C for FEBEX-DP bentonite samples B-C-49-7 (a) and B-C-49-11 (b). The green curve represents the thermogravimetric analysis (left y-axis). The blue curve stands for the DSC analysis (right y-axis). The red dotted line signifies the temperature (2nd right y-axis). (c) and (d); corresponding TGA/DSC curves as a function of time (minutes) for dehydration cycles only at the time interval of the appearance of the second peak or “dehydration shoulder”. See Fig. 7 in the text for explanation of hydration/dehydration cycles. DSC measurements show the peak shifts (A and B) for the dehydration time interval in response to hydration duration.

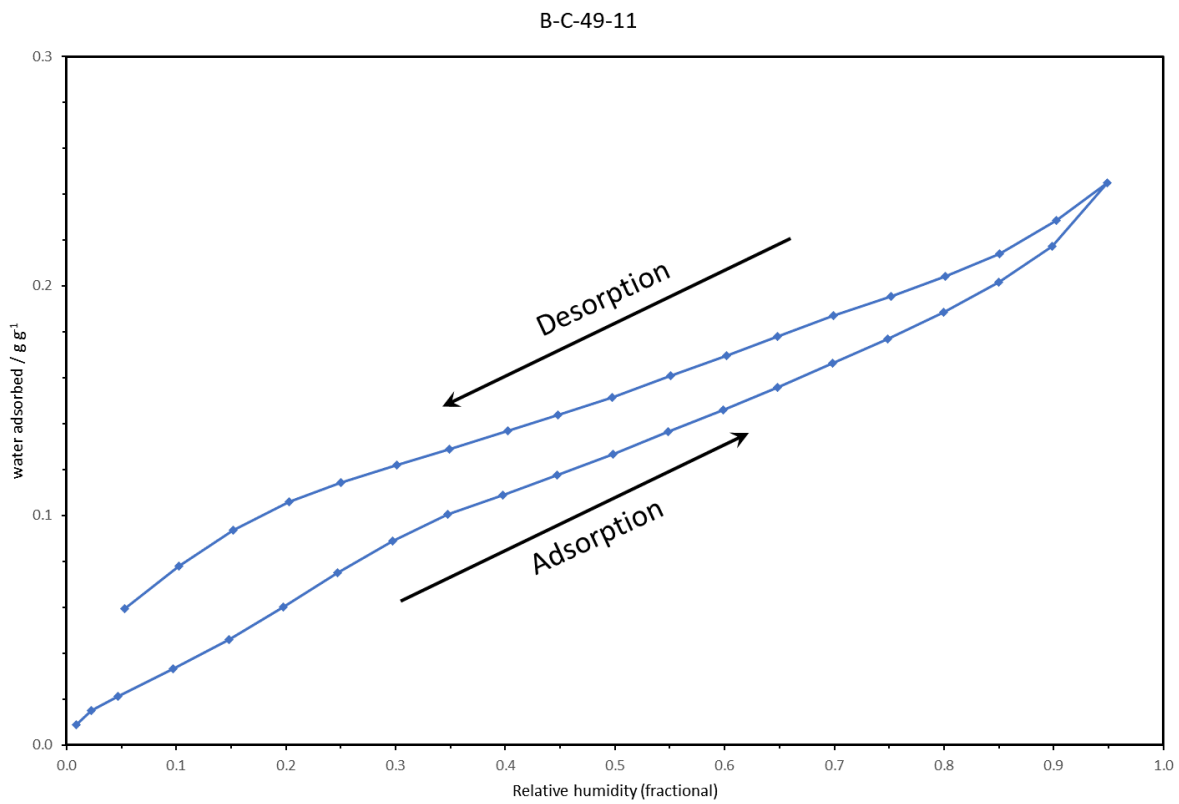
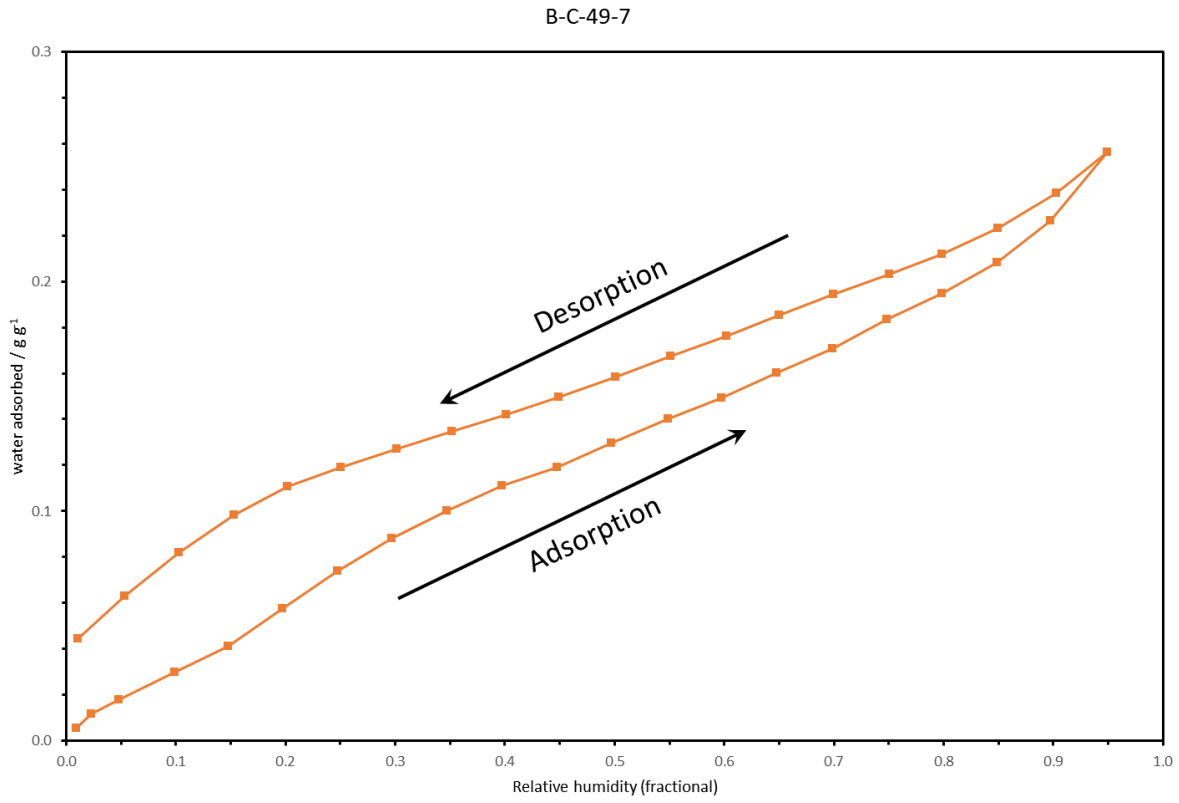


Figure A-5. Volumetric water sorption/desorption isotherms obtained at 20°C for samples BG-C-49-7 and BG-C-49-11.

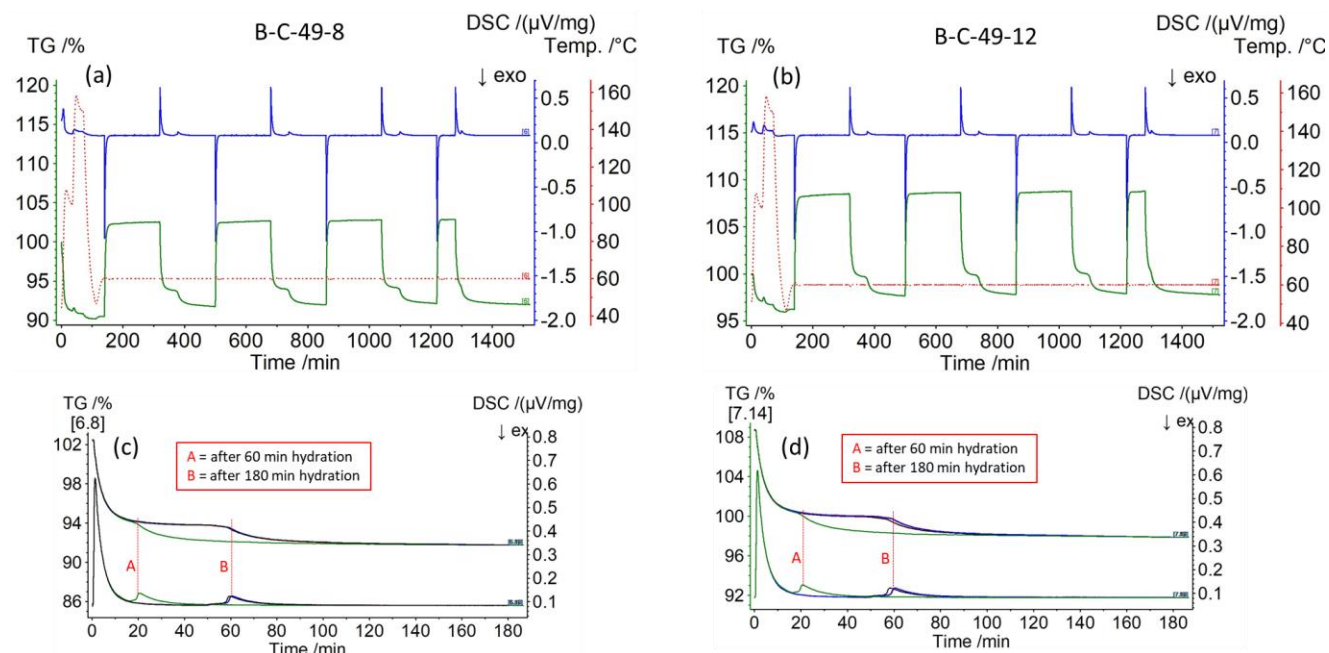


Figure A-6. TGA/DSC curves as a function of time (minutes) for water adsorption/desorption cycles at 60°C for FEBEX-DP bentonite samples B-C-49-8 (a) and B-C-49-12 (b). The green curve represents the thermogravimetric analysis (left y-axis). The blue curve stands for the DSC analysis (right y-axis). The red dotted line signifies the temperature (2^{nd} right y-axis). (c) and (d); corresponding TGA/DSC curves as a function of time (minutes) for dehydration cycles only at the time interval of the appearance of the second peak or “dehydration shoulder”. See Fig. 7 in the text for explanation of hydration/dehydration cycles. DSC measurements show the peak shifts (A and B) for the dehydration time interval in response to hydration duration.

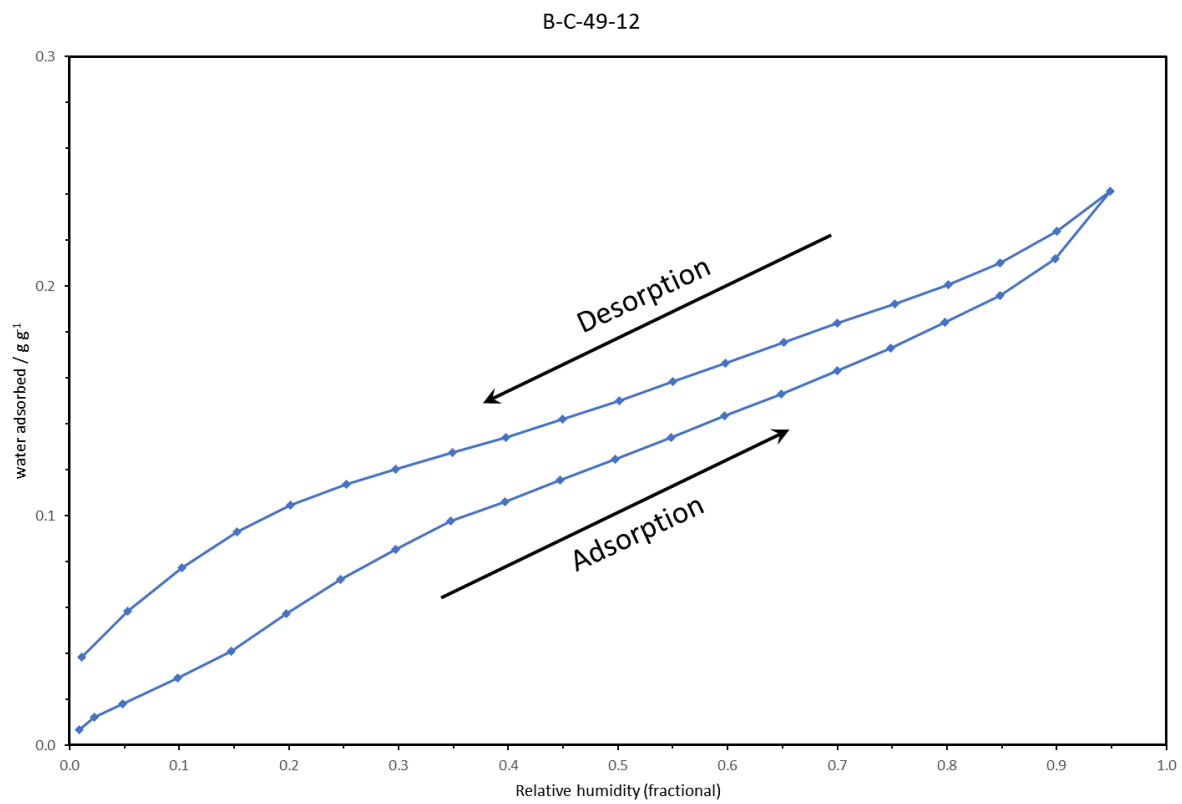
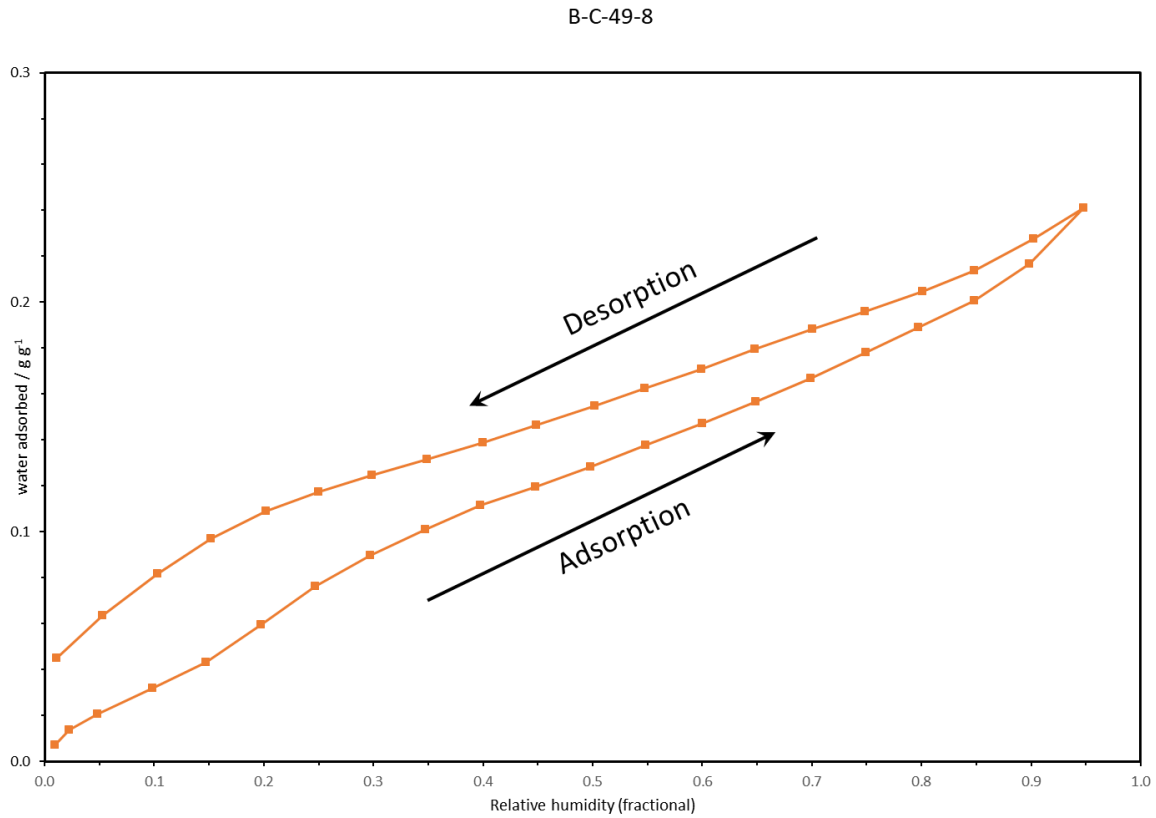


Figure A-7. Volumetric water sorption/desorption isotherms obtained at 20°C for samples BG-C-49-8 and BG-C-49-12.

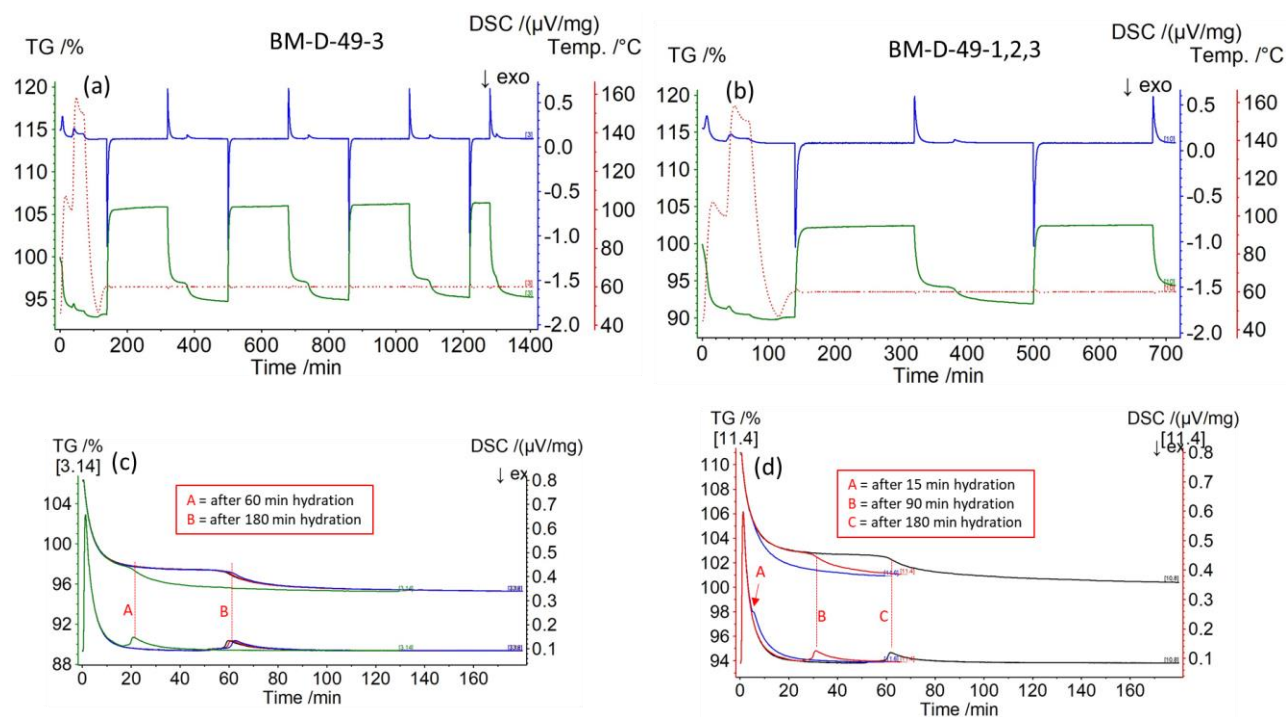


Figure A-8. TGA/DSC curves as a function of time (minutes) for water adsorption/desorption cycles at 60°C for FEBEX-DP bentonite samples BM-D-49-3 (a) and BM-D-49-(1,2,3) (b). The green curve represents the thermogravimetric analysis (left y-axis). The blue curve stands for the DSC analysis (right y-axis). The red dotted line signifies the temperature (2nd right y-axis). (c) and (d); corresponding TGA/DSC curves as a function of time (minutes) for dehydration cycles only at the time interval of the appearance of the second peak or “dehydration shoulder”. See Fig. 7 in the text for explanation of hydration/dehydration cycles. DSC measurements show the peak shifts (A and B) for the dehydration time interval in response to hydration duration.

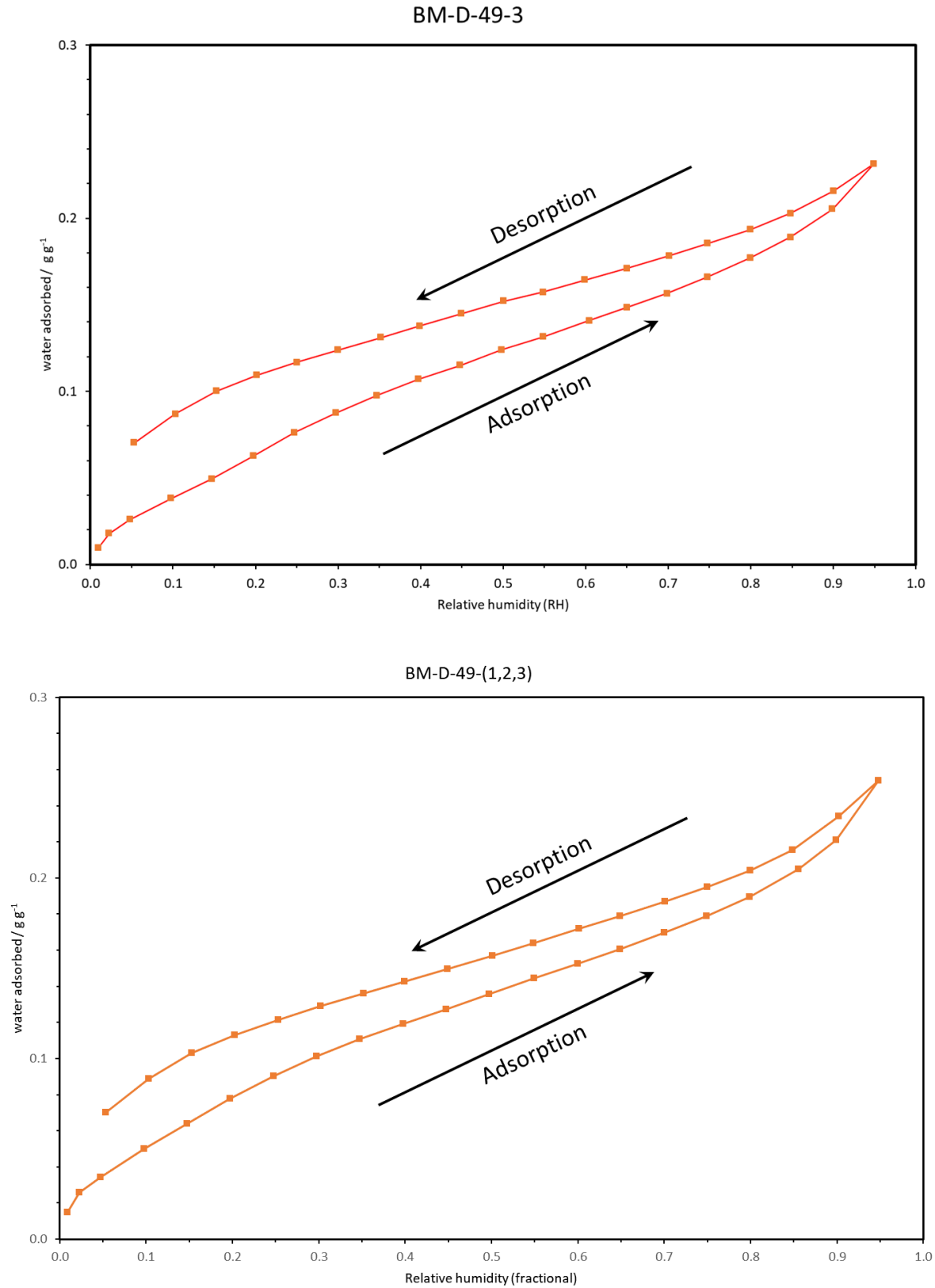


Figure A-9. Volumetric water sorption/desorption isotherms obtained at 20°C for samples BM-D-49-3 and BM-D-49-(1,2,3).